Ecotoxicology and Environmental Safety 292 (2025) 117907

Contents lists available at ScienceDirect

Ecotoxicology and Environmental Safety

journal homepage: www.elsevier.com/locate/ecoenv

Mechanistic insights into microwave radiation induced cognitive impairments: The role of m^6A epigenetic modifications and HNRNPA2B1 in TrkB regulation

Weijia Zhi [a,1], Jiale Tang [b,1], Mingzhao Zhang [a], Yong Zou [a], Simo Qiao [c], Lizhen Ma [a], Ji Dong [a], Binwei Yao [a], Xuelong Zhao [a], Zhenqi Yang [a], Zhongwu Lin [a,d,*], Xiangjun Hu [a,*], Lifeng Wang [a,*]

[a] Beijing Institute of Radiation Medicine, Beijing, China
[b] Changsha Hospital of Traditional Chinese Medicine (Changsha Eighth Hospital), Changsha, China
[c] Beijing Institute of Pharmacology and Toxicology, Beijing, China
[d] National Innovation Institute of Defense Technology, Beijing, China

ARTICLE INFO

Edited by Professor Bing Yan

Keywords:
Microwave
Synaptic plasticity
NSCs
TrkB m^6A modification
HNRNPA2B1

ABSTRACT

Microwave radiation, a prevalent environmental stressor, significantly impacts human health. Based on previous studies, we hypothesize that microwave-induced cognitive impairments and vulnerability in the hippocampal dentate gyrus (DG) region are due to abnormal synaptic plasticity regulated by both newborn and mature neurons derived from neural stem cells (NSCs). Epigenetics links external factors to organisms, offers insights into the health effects of environmental influences. To explore the molecular mechanisms underlying the effects of microwave radiation on neuronal synaptic plasticity from the perspective of mRNA N^6-methyladenosine (m^6A) modification. We first assessed the impact of microwave radiation on cognitive memory abilities in rats through behavioral tests. Immunofluorescence staining were applied to clarify the influence of microwave radiation on both neurons and NSCs. Molecular mechanisms were investigated by ELISA, q-PCR, Western blot, MeRIP-seq, and RNA pull-down experiments. The microwave radiated rat model exhibiting learning and memory deficits. Impaired synaptic plasticity in mature hippocampal neurons alongside hindered NSCs proliferation and development were observed. Using our established non-contact co-culture model, we replicated the *in vivo* adverse effects of microwave radiation. Down-regulated HNRNPA2B1 leads to reduced binding of *TrkB* m^6A and promoted *TrkB* degradation. This feedback loop results in low BDNF expression, ultimately causing cognitive impairments. Our study emphasizes the neurotoxicity of microwave radiation and identifies *TrkB* m^6A modification as a potential target for protecting against cognitive damage induced by electromagnetic radiation.

1. Introduction

The modern world is filled with natural and man-made electromagnetic fields and radiations, which act as stressors and impose increasing burdens on the human biological system (Carpenter, 2013; Lai and Levitt, 2022). Particularly, with the widespread development of communication technology, microwave radiation, commonly refers to electromagnetic waves with frequencies ranging from 300 MHz to 300 GHz, has been widely utilized in various fields such as communication, healthcare, and military. Its adverse effects have gradually attracted attention. Studies have shown that microwave radiation can lead to memory decline, cognitive impairments, and emotional abnormalities (Hao et al., 2023; Jiang et al., 2024; Wang et al., 2022; McCredden et al., 2022; Pall, 2016; Sage and Burgio, 2017).

The hippocampus plays a crucial role in the regulation of emotion and memory (Abe et al., 2024). The DG of the hippocampus, as an

* Corresponding authors.
E-mail addresses: zhi.weijia@163.com (W. Zhi), 19907489199@163.com (J. Tang), zhangmz1919@163.com (M. Zhang), tjuzouyong@163.com (Y. Zou), brenda_echo@sina.com (S. Qiao), malizhen0906487@sina.com (L. Ma), djtjwj@163.com (J. Dong), ybwcsp@163.com (B. Yao), xlong_z@163.com (X. Zhao), yangzq0242@163.com (Z. Yang), linzhw2024@163.com (Z. Lin), xjhu2003@vip.sina.com (X. Hu), fangchang_14@163.com (L. Wang).
[1] These authors contributed equally to this work.

https://doi.org/10.1016/j.ecoenv.2025.117907
Received 19 September 2024; Received in revised form 14 February 2025; Accepted 14 February 2025
Available online 24 February 2025
0147-6513/© 2025 The Author(s). Published by Elsevier Inc. This is an open access article under the CC BY-NC-ND license (http://creativecommons.org/licenses/by-nc-nd/4.0/).

essential component of the hippocampal formation, serves as a significant brain region for adult neurogenesis. In the subgranular zone (SGZ), NSCs continuously proliferate, differentiate into neurons, migrate, and integrate into existing neural circuits, thereby contributing to the regulation of hippocampal cognitive functions in conjunction with mature neurons (Aimone et al., 2006; Gonçalves et al., 2016; Bond et al., 2015). Studies have shown that the hippocampus is a sensitive target of microwave radiation, and impairment of synaptic plasticity in hippocampal neurons is one of the key mechanisms underlying microwave radiation-induced cognitive impairments (Wang et al., 2013; Zhi et al., 2018). Additionally, different doses of electromagnetic radiation can alter the proliferation and differentiation processes of SGZ NSCs in the hippocampal DG region (Cui et al., 2017), for instance, *in vivo* studies utilizing transcranial magnetic stimulation at 1–10 mT found promotion of the proliferation of NSCs in the SGZ of the hippocampus (Leone et al., 2014; Chen et al., 2015; Zhang et al., 2014; Ueyama et al., 2011; Leone et al., 2011); Liu et al. reported that a single exposure of rats to microwave radiation at 9.37 GHz could induce neuronal apoptosis in DG region of the hippocampus and abnormal proliferation of NSCs (Liu et al., 2022). Therefore, we have reason to suspect that the abnormal synaptic plasticity observed in hippocampal neurons, particularly in the DG region, following microwave radiation exposure, is the result of the combined effects of microwave-induced synaptic dysfunction in mature neurons and inhibition of proliferation and differentiation in adult NSCs.

The environment can be viewed as a continuous flow of information from the external world that interacts with the epigenome, activating and continuously altering its molecular and three-dimensional structure. Therefore, epigenetics serves as a suitable tool for studying the interactions between the environment and the organism (Burgio and Migliore, 2015). Epigenetics is a branch of genetics that focuses on heritable changes in gene expression without altering the nucleotide sequence of the genes. RNA methylation has emerged as a hot topic in recent epigenetic research, with m^6A being the most common post-transcriptional modification of RNA in eukaryotes. This modification is carried out by three classes of protein factors: writers, which methylate adenosine at the N^6 position; erasers, which reversibly remove m^6A; and readers, which recognize and bind to m^6A motifs, regulating RNA stability, splicing, transport, and mRNA translation (Readers) (Jiang et al., 2021a). Heterogeneous nuclear (HNRNPA2B1) is one of the nuclear readers of m^6A, stabilizing RNA and promoting protein expression through binding to RNA m^6A sites (Alarcón et al., 2015). Based on a review of the current literature, we note that epigenetic mechanisms play a pivotal role in the regulation of proliferation and differentiation of neural stem cells, while also significantly contributing to the effects of electromagnetic radiation on these cells (Cui et al., 2017; Leone et al., 2014; Kaplan et al., 2006). Brain-derived neurotrophic factor (BDNF) is a critical mediator of activity-dependent processes in the brain. In terms of synaptic plasticity, BDNF is involved in axonal guidance, dendrite and dendritic spine development, and can also modulate long-term potentiation (LTP) induction. In the context of NSCs, BDNF promotes neuronal differentiation and plays a crucial role in the maintenance, proliferation, growth, differentiation, and directed migration of NSCs (Wang et al., 2006). The BDNF/Tyrosine receptor kinase B (TrkB) axis is strictly regulated by epigenetic mechanisms (Mendelsohn and Larrick, 2006). Considering that BDNF may contribute to cognitive impairments following microwave radiation exposure, the role of mRNA m^6A modification in this process remains poorly understood and requires further elucidation.

In the present study, we explored the effects of microwave radiation on the synaptic plasticity of neurons in the hippocampal DG region, which involves the concurrent participation of mature neurons and adult neural stem cells, as well as the underlying mechanism of mRNA m^6A methylation modification. Our findings revealed that down-regulation of HNRNPA2B1-mediated *TrkB* m^6A modification levels resulted in decreased protein expression of TrkB and, consequently, reduced BDNF secretion through feed forward regulation. Additionally, we predicted the potential m^6A methylation modification sites of *TrkB*, providing genetic targets for the prevention and treatment of cognitive impairments resulting from microwave exposure.

2. Methods and materials

2.1. Animals and ethics statement

In this study, male Wistar rats (200 ± 20 g, $N = 90$) were obtained from Wei Tong Li Hua (Beijing, China) and raised at 22–23 °C on a 12-h light-dark cycle (lights on at 7 a.m.). The maintenance feed for rats is procured from SiPeiFu (Beijing, China), which is nutritionally balanced, with a high proportion of readily absorbable components. It meets the daily nutritional requirements of experimental rats and mice beyond the growth and experimental phases. Food and water were freely available. The rats were randomly divided into control and radiation groups, with 45 rats in each group. All protocols were approved by the Institutional Animal Care and Use Committee of Beijing Institute of Radiation Medicine. License number IACUC-DWZX-2020-648.

2.2. Cell preparation

2.2.1. Culture of primary hippocampal neurons

Wistar rats at postnatal ages of younger than 12 h were purchased from Wei Tong Li Hua (Beijing, China). All protocols were approved by the Institutional Animal Care and Use Committee. Primary hippocampal neuron cultures were prepared as described in Supplementary material. The cells were randomly divided into the control group (Con) and the exposure group (Exp).

2.2.2. Neural stem cell culture and passaging

The primary culture and passaging of rat hippocampal NSCs was carried out as described by Gage et al. (Li et al., 2006; Gage et al., 1995; Afhami et al., 2023). Briefly, the hippocampal tissue was isolated and pancreatic enzyme digestion was performed. The cell suspension was filtered and centrifuged at 1000 rpm for 5 minutes. Then the cells were seeded at a density of 1×10^6/ml in T25 culture flasks and incubated in a CO_2 incubator. On the second day after seeding, complete medium replacement was performed. Subsequently, half-medium replacement was performed every day. The medium composition was as follows: DMEM/F12 medium (48 ml, 96 %), N2 (0.5 ml, 1 %), B27 (vitamin A-free, 1 ml, 2 %), penicillin-streptomycin solution (100 × dilution, 0.5 ml, 1 %), EGF (20 ng/ml), and bFGF (20 ng/ml). Passaging was performed approximately every 5 days. The detailed operational steps of the above procedures can be found in the Supplementary materials.

2.2.3. Co-culture model of primary hippocampal neurons and NSCs

To establish a co-culture model of primary hippocampal neurons and NSCs, the following experimental procedure was conducted: First, the isolated hippocampal neurons were prepared as a suspension and seeded at a density of 1×10^6/ml onto poly-L-lysine-coated 35 mm culture dishes/petri dishes. After approximately 4 h of incubation, the seeding medium was aspirated and replaced with 2 ml of feeding medium. On the second day, half of the culture medium was replaced, and the culture dishes were placed in a CO_2 incubator for continued cultivation. After 1–2 days of primary hippocampal neuron culture, the petri dish was taken out, and the primary hippocampal neurons, along with NSCs cultured to the 3rd generation, were separately seeded into the upper and lower compartments of a Transwell insert. The Transwell insert had a semi-permeable polycarbonate membrane with a pore size of 0.4 μm, which prevented cell migration while allowing the passage of culture medium components (Smith et al., 2015). The entire co-culture system with corresponding medium (the formula can be found in the Supplementary materials) was placed in a CO_2 incubator for co-cultivation. The choice of which layer to seed the neurons and NSCs in the Transwell insert depended on the experimental objectives: when analyzing NSC

development, NSCs were seeded in the lower compartment and primary hippocampal neurons in the upper compartment; when analyzing neuronal synaptic plasticity and molecular mechanisms, primary hippocampal neurons were seeded in the lower compartment and NSCs in the upper compartment (using passaged culture medium suspension). Photographic records were taken at 1, 3, 5, and 7 d of co-culture to document the growth status of the NSCs.

2.3. Microwave exposure and dosimetry

The microwave exposure system was based on a klystron amplifier, model JD 2000 (Vacuum Electronics Research Institute, Beijing, China). Square wave pulses of 2.856 GHz microwave were applied for 3 * 6 min per day for 4 days, with an interval of 6 min between each exposure, with a peak power density of 200 mW cm^{-2}, the mean of the power densities for the area was 30 mW cm^{-2}, repetition frequency 300 Hz, and duty Cycle 0.015 %. Rats in the microwave exposure group were placed in a metal-free fanshaped container made of porous plexiglass. The container was placed on a circular platform directly below the microwave horn antenna. Rats in the control group were processed in parallel with those in the microwave exposure group, but the microwave source was switched off. For cell exposure, cells in the control group were processed in parallel with those in the microwave exposure group, while the microwave source was switched off. The SAR of the cells was determined numerically using the simulated software package Empire V4.10. The medium model with meniscus was based on the profile functions of Schuderer and Kuster (2003).

2.4. Optic fiber thermometry

The rectal temperature of the rats were monitored in real time during microwave exposure using a fiber optic thermometer (model THR-NC-1084C, FISO, CA). Briefly, rats were raised in cages with-out padding or other edible items. The solid feed was replaced with 10 % sucrose water solution 7 d before the treatment to eliminate the influence of feces in the rectum on temperature detection. Rats were then fixed in a special holder made of acrylic material, placed on the microwave exposure platform. To obtain the average level of anal temperature change of all rats, one of the temperature measuring rats was placed parallel to the direction of E-polarization and the other was placed perpendicular to the direction of E-polarization. Due to the limits of the temperature measuring device, the whole process is repeated twice. A metal-free fiber optic thermometer sensor (2 mm diameter) was inserted into the anus with a depth of ≈ 1 cm. Temperature data were transmitted through the optical fiber and recorded before, during, and after microwave exposure. Upon assessing the thermal conditions of cells, the culture dish was precisely positioned at the central locus of the exposure platform.

2.5. Assessment of the learning and memory abilities of rats

2.5.1. Spatial learning and memory

The Morris water maze (MWM) was applied in this study to assess the spatial learning and memory abilities of the animals. The navigation test was used to test the spatial learning ability of the animals and was carried out 1–6 d after microwave radiation. The rats were placed in each quadrant of the pool from a fixed entry point in each experiment, and a timer was started. If the rat could find the platform within 60 s, the timer was stopped, and the rat was allowed to stay on the platform for 15 s; if the rat failed to find the platform after 60 s, it was guided to the platform and allowed to remain there for 15 s. The average escape latency (AEL) of each rat was calculated as the average time required to find the platform among the four quadrants. After 8 days of microwave radiation (9 d), the probe test was carried out to evaluate the spatial memory ability of the rats; the platform was removed from the pool, and the other conditions were kept constant. The rats were placed in the pool in quadrants 2, 3 and 4, and the time spent swimming in the quadrant where the platform was originally located and the number of times the original platform area was crossed within 60 s were recorded.

2.5.2. Event memory

Rats underwent the novel object recognition test 2 days after the MWM test was finished. The experimental apparatus included a 1000 mm × 1000 mm × 400 mm opaque black box; a camera was placed above the open box, and the space above the box was covered with a curtain to keep the light uniform and soft. On the 10th and 11th days after exposure, the adaptation experiment was carried out for 10 min. The box was wiped with 75 % alcohol after each experiment to prevent residual odor from interfering with the results of subsequent experiments. The learning and test experiments were carried out on the 12th day after exposure. During the learning experiment, two identical red cylinders (old objects) were placed in the open box at 1/3 of a diagonal line, and the time the rats spent exploring (i.e., touched the object with their head or forelimb) the cylinders within 10 min was recorded. The test experiment began an hour after the learning experiment ended; one of the red cylinders was randomly selected and replaced with a green cone (novel object), and the time that the rats spent exploring the cone and cylinder within 5 min was recorded. The event memory ability of rats was evaluated by calculating the discrimination index using the formula below:

$$\text{Discrimination} = \frac{\text{TimeExploreNovelObjects} - \text{TimeExploreOldObjectes}}{\text{TotalExplorationTime}}$$

All animal movements and behaviors were recorded by VisuTrack software.

2.6. Transmission electron microscopy of rat hippocampal tissue

At 6 h, 7 d, 14 d and 28 d after exposure, 3 rats from each group were anesthetized by intraperitoneal injection of 1 % pentobarbital sodium, and a 1 mm^3 cube was dissected from the left hippocampal DG of each brain. Sections were prepared as described previously (Zhi et al., 2018). Briefly, after fixation in 2.5 % glutaraldehyde (Merck, Darmstadt, Germany), the samples were incubated with 1 % osmium tetroxide (AppliChem, Gatersleben, Germany) and graded ethyl alcohol solutions and then embedded with EPON618 (TAAB Laboratories Equipment, Berks, UK). The sections were placed on copper mesh and stained with uranyl acetate and lead citrate (Advanced Technology & Industrial Co. Ltd, Hong Kong, China) for contrast. After drying, the specimens were observed under a transmission electron microscopy (TEM) (H-7650, Tokyo, Japan).

For each sample, visual fields containing Gray's type I synapses (with typical asymmetry of the presynaptic and postsynaptic membranes and more vesicles in the presynaptic membrane) were randomly selected for imaging, ensuring that at least 15 Gray's type I synapses were analyzed (at least 15 photos were captured) for each group at each time point. The length and thickness of the postsynaptic density (PSD) were measured by Image J software (URL: https://imagej.en.softonic.com), and the values were recorded.

2.7. Timm staining

Rats were exposed to microwave radiation, and the MWM test was conducted as reported previously (Zhi et al., 2018). At 6 h, 7 d, 14 d and 28 d after radiation, 2 rats that had been trained in the MWM were chosen from each of the control and radiation groups, weighed, and anesthetized with 1 % pentobarbital sodium. Subsequently, heparin/*PBS* solution, 0.4 % sodium sulfide solution and 4 % paraformaldehyde solution (pH 7.0) were perfused through the left ventricle. Brain tissue was isolated and successively placed in 20 % and 30 % sucrose solution for dehydration until the tissue sank to the bottom.

Coronal sections were obtained using a cryotome, stained with a mixture of 50 % gum arabic, citrate buffer, 5.6 % benzene diphenol and 17 % silver nitrate for 20–30 min in the dark, washed with distilled water for 15 min, dehydrated with alcohol and xylene, cleared in xylene and blocked with gelatin. Images were obtained using a bright field microscope (Axioscope 5, Carl Zeiss, Germany).

2.8. BrdU administration

Twelve rats were randomly selected from each group. To investigate how microwaves affect the proliferation, differentiation, and migration of NSCs, during the radiation exposure period, BrdU (50 mg/kg) was intraperitoneally injected into the mice twice a day, i.e., in the morning (1 h before radiation) and at night, at an interval of 12 h. At 6 h, 7 d, 14 d and 28 d after radiation exposure, the brains of 3 rats in each group were perfused with paraformaldehyde, and frozen sections were prepared.

2.9. Immunostaining and image analysis of primary neurons

The slices which mounted frozen sections were placed in a staining box containing 0.3 % PBS-Triton solution and incubated for 35 min. Hydrochloric acid (2.0 N) was added dropwise to the brain slices and incubated at 37 ℃ for 35 min. Then, the slices were washed with borate buffer and blocked at room temperature for 1 hour. They were then incubated with primary antibodies at 4 ℃ overnight. Then, the slices were washed in PBS and incubated with secondary antibody at room temperature for 1 h. The nuclei were counterstained with 4′, 6-Diamidino-2-phenylindole (DAPI) (VECTASHIELD Antifade Mounting Media, Vectorlabs, USA); images were captured with a fluorescence microscope (Axioscope 5, Carl Zeiss, Germany) or Confocal (LSM 980ZEISS, Carl Zeiss, Germany). The antibodies used in the immunofluorescence experiment could be seen in Supplementary materials.

To ascertain dendritic complexity, which encompasses the determination of total dendritic length, terminal dendritic length, and the degree of dendritic branching, Sholl analysis was performed utilizing the Image J plugin (Binley et al., 2006). This analytical approach involved placing a central point on the soma and tracing concentric circles with a radial increment of 10 μm. Each instance where a dendritic branch intersected a circle was recorded (Binley et al., 2006). For dendritic spine analysis, the length of each dendritic segment was measured, and the number of dendritic spines was manually tallied. Spine density was calculated by dividing the total spine count by the length of the dendritic segment. For each group and at each time point, images of 15 neurons were captured, and three dendritic segments per neuron were selected for analysis (Ferreira et al., 2014). To evaluate the propensity of NSCs to differentiate into mature neurons or astrocytes within a co-culture model comprising primary hippocampal neurons and NSCs, we conducted semi-quantitative analysis of the fluorescence intensity. The predilection of NSCs within neurospheres to differentiate into mature neurons or astrocytes is represented by the following formulas:

$$\text{Differentiation index towards } \textit{Neurons} = \frac{\textit{Integrated Density of NeuN}}{\text{Integrated Density of DAPI}}$$

$$\text{Differentiation index towards } \textit{Glial Cells} = \frac{\text{Integrated Density of } \textit{GFAP}}{\text{Integrated Density of DAPI}}$$

To characterize and evaluate the purity and cellular state of NSCs within neurospheres, we employed the aforementioned differentiation propensity indices. These indices provide a quantitative measure of the inclination of NSCs to undergo maturation into specific neural lineages when subjected to defined co-culture conditions.

2.10. Total RNA isolation and real-time RT—PCR

Total RNA was isolated from the left hippocampus of 5 rat brains with TRIzol at 6 h, 7 d, 14 d and 28 d after microwave exposure, and the RNA was then reverse transcribed using a RevertAid first-strand cDNA synthesis kit (Thermo Scientific, USA). For each sample, the experiment was conducted 3 times. Real-time RT—PCR was carried out using a thermocycler (Applied Biosystems 7300 Real-Time PCR System, USA). The reaction parameters were as follows: predenaturing at 95 ℃ for 10 min, followed by 40 cycles of denaturing at 94 ℃ for 10 s, annealing at 56 ℃ for 20 s and 68 ℃ for 35 s. The GAPDH gene was used as the internal reference. Relative expression was calculated by comparing target gene expression in the experimental group with that in the control group, and these values were statistically analyzed. The primer sequences can be found in the Supplementary materials.

2.11. Protein extraction and western blot

The hippocampal tissues used for this experiment were the same as those used for RNA extraction. The samples were homogenized in 200 μl RIPA lysis buffer (Applygen Technologies, BJ, China) supplemented with 1 % (v/v) protease inhibitor cocktail (Selleck Chemicals, USA) and lysed for 45 min on ice. Then, the samples were centrifuged at 12,000 rpm for 15 min at 4 ℃. The protein concentrations were measured by the bicinchoninic acid (BCA) assay (Roche Applied Science). Then, the protein extracts were diluted in 4 × sample buffer and denatured for 10 min at 100 ℃. Western blotting was performed as described previous (Zhi et al., 2018), and 30 μg protein was loaded in each lane of the gel. The primary antibodies were purchased from Abcam. The dilution ratios were as follows: anti-BDNF antibody: 1:1000; anti-TrkB: 1: 5000; anti-HNRNPA2B1: 1: 1000 and anti-GAPDH antibody: 1:10000. The bands were visualized by an enhanced chemiluminescence detection system, and the densities of the target bands were analyzed by normalization to the density of the GAPDH band from the same sample. For each sample, the experiment was conducted 3 times.

2.12. Enzyme linked immunosorbent assay (ELISA)

Detection of BDNF protein in rat hippocampal neurons after microwave radiation was performed using an enzyme-linked immunosorbent assay (ELISA) (Rat BDNF ELISA Kit, E-EL-R1235, Elabscience, China) according to the manufacturer's instructions. The detailed procedures can be found in the Supplementary materials.

2.13. Cell counting Kit-8 (CCK-8) assays

To assess the proliferation capacity of NSCs after microwave radiation, we employed the CCK-8 assay (bimake, China) to evaluate NSCs proliferation. After microwave radiation, the third-generation NSCs were collected and re-seeded into a 96-well plate. For specific procedural steps, please refer to the Supplementary materials. On the 1, 3 and 5 days after radiation, cells were retrieved for the experiment, with 5 wells per group and 3 wells serving as negative controls without cells. 10 μl of CCK-8 solution was added to each well, followed by incubation in the cell incubator for 1.5–2 h. Finally, the absorbance at 450 nm was measured using a microplate reader (Spectra Max 190, Molecular Devices, USA). The absorbance value of each well was subtracted by the average value of the negative control group, yielding the OD value.

2.14. Quantification of m^6A methylation levels

The level of total RNA m^6A methylation in rat hippocampal tissues was measured according to the manufacturer's instructions, EpiQuik m^6A RNA Methylation Quantification Kit (Colorimetric) (P-9005, Epigentek, USA); for each sample, the experiment was conducted 3 times. The relative content of m^6A was calculated from the obtained absorbance values.

2.15. Methylated RNA immunoprecipitation sequencing (MeRIP-seq)

Total RNA of primary hippocampal neurons at 0 h post microwave

radiation was isolated and purified using TRIzol reagent (Invitrogen, Carlsbad, CA, USA) in accordance with the manufacturer's protocol. Following this, the RNA was subjected to quantification and further purification. After assessing and confirming the integrity of the RNA, it was fragmented, and then m^6A antibodies were utilized to enrich the RNA containing m^6A modifications. The enriched RNA fragments were subsequently reverse transcribed to construct a cDNA library. The constructed library was subjected to quality control and, upon passing the quality assessment, underwent sequencing. Subsequently, a series of relevant bioinformatics analyses were performed. Detailed procedural steps can be found in the Supplementary materials.

2.16. RNA pull-down assay, silver staining, and mass spectrometry (MS)

During the RNA pull-down experiment, cell pellets were lysed in IP lysis buffer and incubated on ice. Total proteins were obtained through centrifugation, with 100 μl reserved as the input sample. Target RNA was then bound to streptavidin-coated magnetic beads, followed by washing and incubation with biotin-labeled RNA to facilitate RNA binding. Protein-RNA complexes were formed by mixing the beads with a protein solution and incubating at 4 °C. The complexes were eluted, and RNA purification was performed using Trizol. The following primer sequences were utilized: *NTRK2*-biotin-1, *NTRK2*-biotin-2, and NC probe.

Purified RNA underwent silver staining, followed by electrophoresis. The resulting gel was fixed, sensitized, stained, and developed to

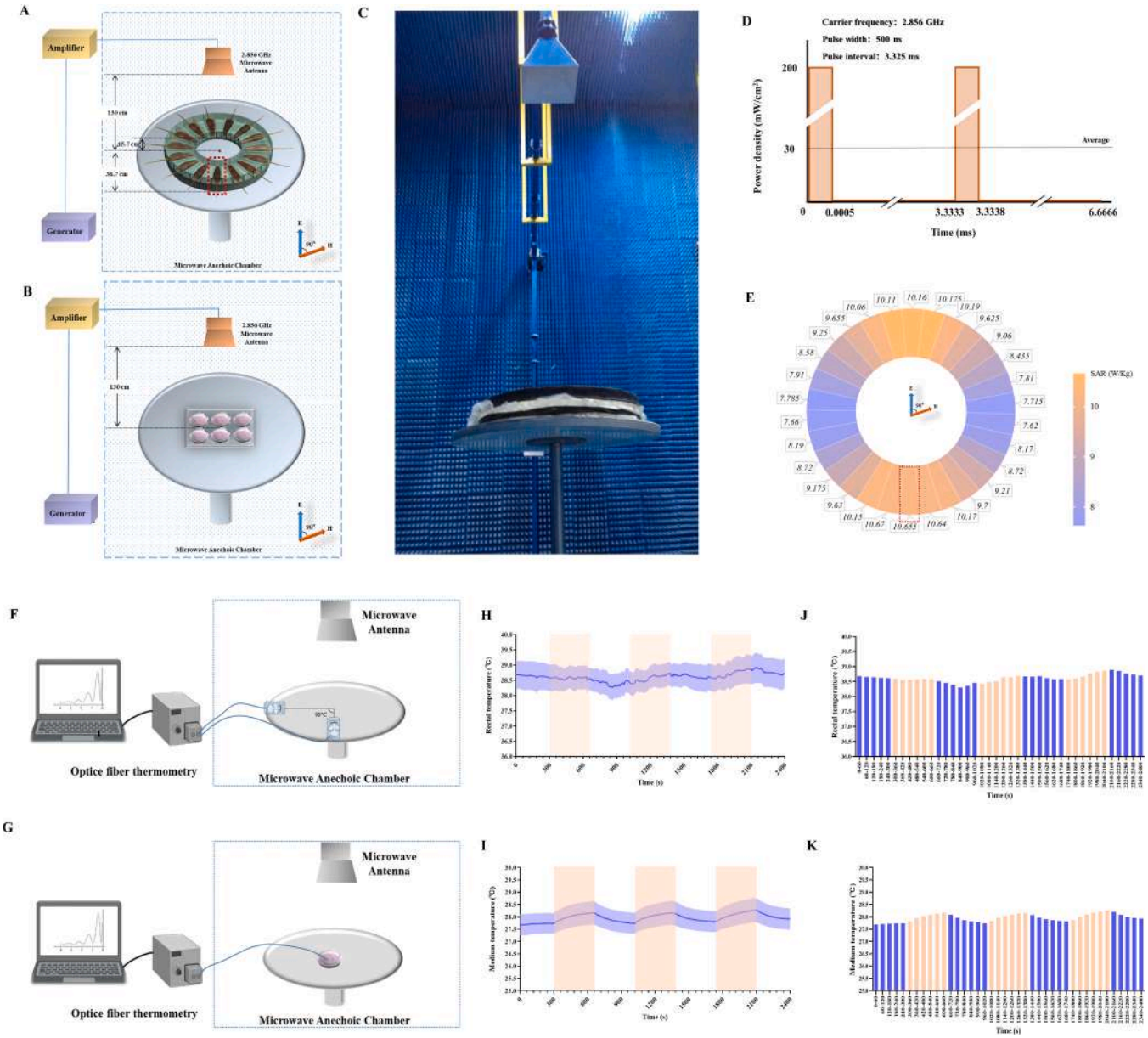


Fig. 1. Microwave exposure system and changes in rat rectal temperature. A–C: Schematic and photos of the microwave exposure system. D: Microwave modulation. E: The distribution of SAR for each rat in the radiation container. F and G: Schematic of the experimental device. Rectal and culture medium temperature measured by an optic fiber thermometer (n = 4 rats or 4 petri dishes). H and I: Plot of average rectal/medium temperature before, during, and after microwave exposure. The purple shadow along with the plot indicates the standard error of the mean (SEM), the orange shadow indicates the phase in which the microwave source is turned on, the rest is the period when the microwave source is turned off. J and K: Histogram of rectal/medium temperature. Each column represents the rectal temperature average of four biological replicates every 60 s. The orange column denotes the "on" stage of the microwave source, and the purple column denotes the "off" stage. E: E-polarization, H: H-polarization.

visualize the RNA. The sample was then prepared for mass spectrometry analysis by denaturing, reducing, and alkylating the proteins in a reaction buffer, followed by trypsin digestion and desalting. Mass spectrometry was performed using a Q Exactive HF mass spectrometer coupled with UltiMate 3000 RSLCnano liquid chromatography, and data were analyzed using MaxQuant software with the Andromeda algorithm. Details see in Supplementary materials.

2.17. Statistical analysis

SPSS 19.0 software was used to analyze the experimental data. $\bar{x} \pm s$ statistically described data with a normal distribution. For quantitative group data, the *t*-test was utilized. To compare various groups of data, one-way analysis of variance was performed. If the difference between groups was statistically significant. Dunnett's *t*-test was employed to compare the difference between the two groups. Data that did not conform to the normal distribution were statistically described by median quartile distance and statistically evaluated by Mann-Whitney *U* test and Kruskal-Wallis test. Repeated-measures analysis of variance was used to analyze the AEL in the MWM test. All differences were examined using a bilateral test, and the test level was $p < 0.05$ (*, $p < 0.05$, **, $p < 0.01$). All graphs were generated by GraphPad Prism 5.02 software.

3. Results

3.1. Microwave exposure causes less than 1 °C increase both in vivo and in vitro

The MW exposure device applied in this study is shown in Fig. 1, A–C. The sizes of the antenna were 140 mm * 110 mm * 160 mm, and the distance between the antenna and the container was 130 cm, far-field distance was 70.2 cm. The rats were fixed in a fanshaped metal-free box, the direction of polarization is parallel to the rat circled by the red dotted line and at an angle to the rat in other positions. The microwave had a carrier frequency of 2.856 GHz, with 300 Hz square modulation and a duty cycle of 0.015 % Fig. 1, D. The peak power density at the platform center was 200 mW cm^{-2} and the average power density was 30 mW cm^{-2}. The whole-body SAR of each rat was calculated and visualized as in Fig. 1, E. The maximum SAR value was 10.655 W/kg, which was at the location of the rat along with the E-polarization. The rectal temperature of the mice was monitored during the microwave radiation treatment using optic fiber thermometry (Fig. 1, F). The rectal temperature baseline of rats was 38.68 ℃, measured under ambient temperature of 23.2 ℃ and 62 % humidity. The rectal temperature of rats decreased 0.11 ℃ before radiation, which may have been caused by the heat exchange between rats and the environment. When the microwave source was turned on, during the 3 * 6 min (360 s) of microwave exposure, the rectal temperature increased by 0.33 ℃ at most compared to the initial temperature at the beginning of radiation period, then it fell back when the source was turned off (Fig. 1, H and J). This showed that exposure to 2.856 GHz microwave radiation with an average power density of 30 mW cm^{-2} applied for 3 * 6 min with a 6 min interval between each exposures caused less than 1 ℃ increase in rectal temperature. For cells, the microwave exposure device and parameters were consistent with those used for rat exposure, with the only difference being that in the microwave exposure and optical fiber temperature measurement experiments, the cell culture dishes were placed at the center of the exposure platform (Fig. 1, F). Similarly, in the cell exposure experiment, we did not observe a temperature increase greater than 1 ℃ in the cell culture medium, as shown in Fig. 1, I and K. The baseline temperature of the cell culture medium before the exposure was 27.68 ℃, and the ambient temperature was 22.4 ℃ with a humidity of 59 %. Upon turning on the microwave source, during the 3 * 6 min (360 s) of microwave exposure, the temperature of the culture medium increased by a maximum of 0.58 ℃ compared to the starting radiation, and the liquid temperature returned to normal after turning off the microwave source.

3.2. Rats exposed to microwave radiation exhibited a decline in learning and memory capabilities

The timeline for the behavioral experiments conducted post-treatment is delineated in Fig. 2A. At 1–6 days following microwave radiation, the navigation test of the MWM test was conducted, and the probe test was carried out 8 days after microwave radiation (Fig. 2, B and C). For the novel object recognition test, the rats were adapted to the apparatus for 10 min on 10th and 11th days after radiation, and the learning and test experiments were performed on the 12th day after exposure. Data pertaining to the MWM test are presented in Fig. 2, D–H. In the place navigation trials, no significant disparities were observed in the swimming velocities between the control and radiated cohorts ($n = 15$) (Fig. 2, D), suggesting that the locomotor capabilities of the rats were not substantially impaired by microwave radiation. During the navigation phase, the exposed group exhibited a notably prolonged average escape latency (AEL) compared to the control group on days 5 and 6 post-exposure ($p < 0.01$), with an aggregate analysis revealing a substantially increased AEL in the radiated rats relative to controls ($n = 15$, $p < 0.05$) (Fig. 2, E). This increment is indicative of a spatial learning deficit subsequent to microwave exposure. In the spatial probe trials, the exposed rats demonstrated a significant reduction in both the number of platform crossings and the duration spent in the target quadrant in comparison to the control group ($n = 15$, $p < 0.01$ or $p < 0.05$) (Fig. 2, F and G), signifying a compromised spatial memory capacity post-exposure.

Assessment of episodic memory abilities in rats was carried out utilizing the novel object recognition (NOR) test, with results delineated in Fig. 2, H. The recognition index in the radiated group was markedly inferior to that of the control group ($n = 15$, $p < 0.05$), implying a detriment to episodic memory functions in rats following microwave exposure.

3.3. Rat hippocampal neurons exhibit abnormal synaptic plasticity after microwave radiation

To elucidate the effects of microwave exposure on synaptic plasticity within the hippocampal DG region of rats, we integrated TEM with Timm staining for a comprehensive evaluation. Given that dendritic spines are integral to the constitution of the postsynaptic components of synapses, the assessment of PSD length and thickness via TEM examination of hippocampal DG brain tissues provided insights into the morphological traits at the termini of dendritic spines. Representative TEM images of hippocampal PSDs and their corresponding quantitative analyses are depicted in Fig. 3B and E. Our findings reveal that, at both 6 h and 14 days following microwave radiation, the PSDs within the hippocampal DG of the radiated subjects exhibited a significant diminution in length and thickness relative to the control group ($n \geq 15$, $p < 0.05$ or $p < 0.01$). These observations indicate that microwave exposure precipitates atypical plasticity in dendritic spines, manifesting as a predilection for immature spine morphological configurations.

It is well documented that the majority of nascent neurons emerging in the subgranular zone (SGZ) of the hippocampal DG are assimilated into the prevailing DG circuitry within a three-week period, directing their axons through mossy fiber tracts towards the CA3 region and establishing excitatory synaptic connections via the perforant pathway (Li et al., 2006). Hence, some axonal constituents within the mossy fibers are derived from these newly generated neurons. Accordingly, should microwave exposure result in the inhibition of mossy fiber sprouting, it could be inferred that microwave exposure also undermines the proliferative potential of newly formed neurons as well as their capacity to act as presynaptic elements in synapse formation with dendritic spines of other neurons. Post-learning and memory assay, visualization of mossy fiber sprouting within the hippocampal DG

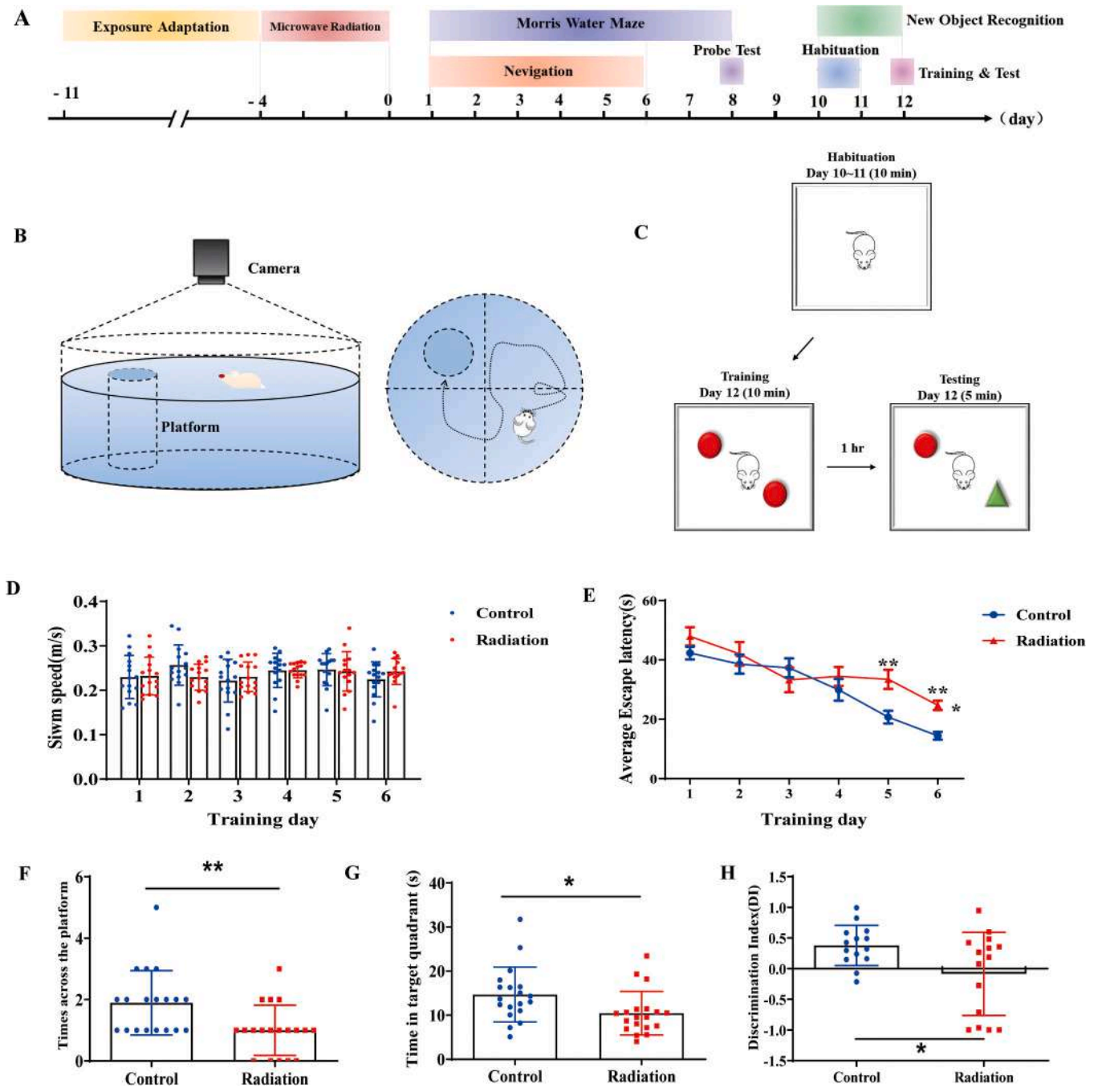


Fig. 2. Effects of microwave radiation on spatial memory and event memory in rats. A: Time schedule of the behavioral experiment. The rats received adaptive training for 7 days before exposure, followed by 4 consecutive days of microwave exposure. B: Schematic diagram of MWM test. C: Schematic diagram of new object recognition experiment (the red circle represents the cylinder old objects and the green triangle represents the cone novel object). D: The swimming speed of the rats in the two groups was not significantly different (n = 15). E: The AEL of the rats in the navigation test; the AEL in the control group was much shorter than that in the radiation group (n = 15). F: The rats in the radiation group crossed the platform fewer times during the probe test than the rats in the control group (n = 15). G: The time spent swimming in the target quadrant in the probe test was shorter in the radiation group than in the control group (n = 15). H: Graph of the discrimination index of the rats in the novel object recognition experiment after microwave radiation exposure (n = 15). Data are presented as mean ± SEM. Repeated-measures analysis of variance was performed to analyze the repeated measurement data (D and E). Student's *t*-test was performed to compare the differences between two groups (F–H). *, $p < 0.05$; **, $p < 0.01$.

extending into the CA3 region was documented (Fig. 3, F). The radiated group exhibited a markedly reduced volume of mossy fiber sprouting in comparison to the control group; quantitative assessments corroborated a substantial disparity in the volume of mossy fiber sprouting at both 14 and 28 days post-radiation (n ≥ 5, $p < 0.05$) (Fig. 3G).

3.4. The proliferation and differentiation of NSCs in the hippocampus were suppressed by microwave radiation

In the present experiment, the proliferation of cells in the SGZ of the hippocampal DG post-microwave exposure was evaluated by quantifying the number of BrdU-labeled newly born cells and Ki67-marked mitotic cells (Fig. 4, B). At all examined time points following

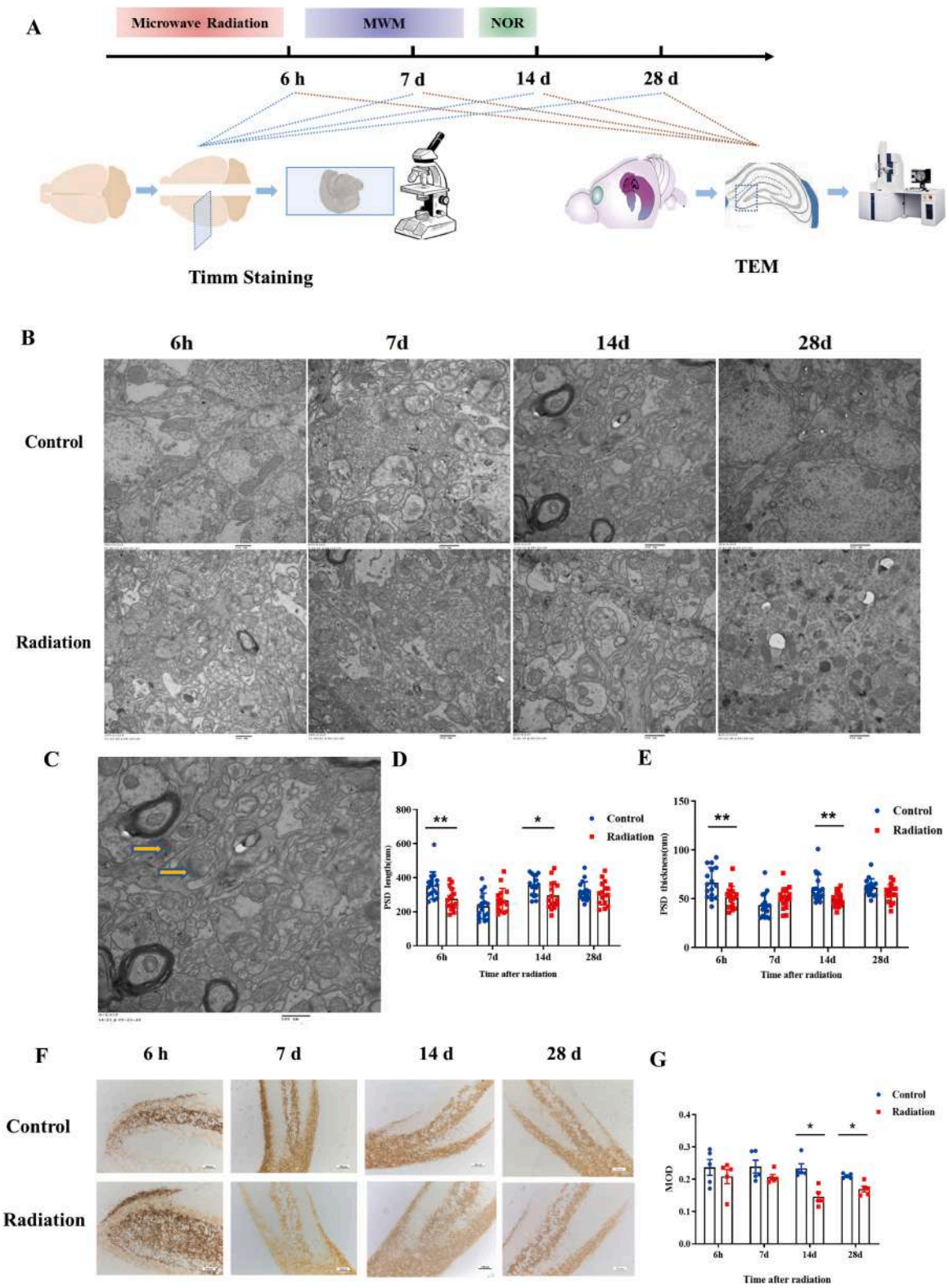
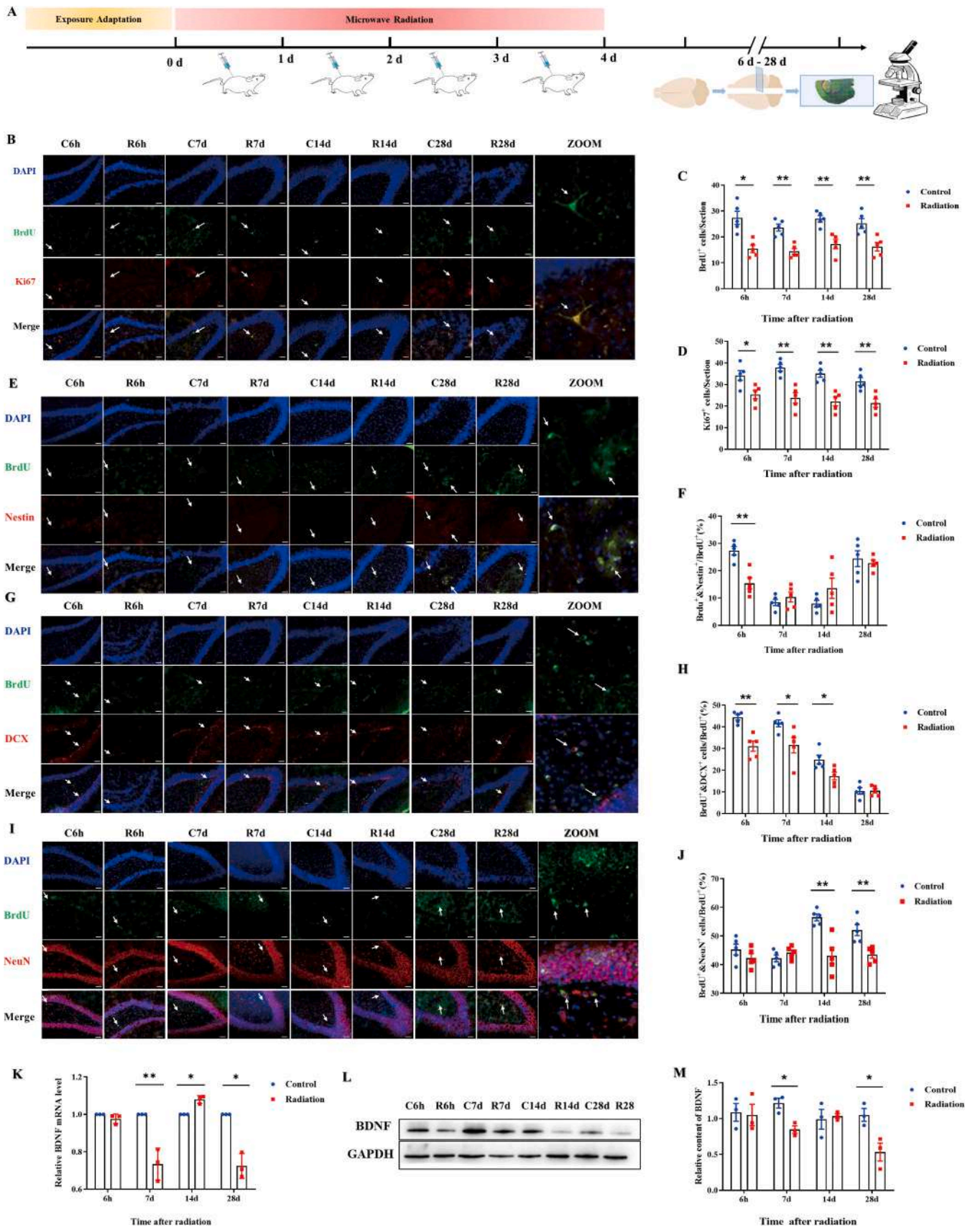


Fig. 3. Alterations of synaptic structure in DG region of hippocampus after microwave radiation. A: Schematic diagram of TEM and Timm staining procession. B: Ultrastructural images of synapses in the hippocampus of rats in the control and radiation groups at 6 h, 7 d, 14 d and 28 d after microwave radiation exposure (Con: control group, Rad: radiation group, scale bar = 500 nm). C: Representative ultrastructural image of Gray's type I synapses in the rat hippocampus: typical asymmetry of the presynaptic and postsynaptic membranes and more vesicles in the presynaptic membrane were observed (the image is a magnified version of the image in Fig. 3 of a synapse in the control group at 14 d; A, the yellow arrows indicate the PSDs). D and E: PSD length and thickness in the rat hippocampus after microwave radiation exposure (n ≥ 15 from 3 rats' hippocampi). F: Images of the microstructure of sprouted mossy fibers in the rat hippocampus at each time point (the blue arrows show the growth of mossy fibers, scale bar = 100 μm); G: Quantitative analysis of mossy fiber sprouting in the rat hippocampus after microwave radiation exposure (n ≥ 5 from 3 rat hippocampi). Data are presented as mean ± SEM. Student's *t*-test was performed to compare the differences between two groups per time point (D, E and G). *, $p < 0.05$; **, $p < 0.01$.



(caption on next page)

Fig. 4. NSCs proliferation and differentiation were attenuated after microwave exposure. A: Schematic diagram of BrdU administration and observation time point. B: Immunofluorescence staining of $BrdU^+$ and $Ki67^+$ cells in the DG region of the hippocampus in the control and radiation groups. C and D: Numbers of $BrdU^+$ and $Ki67^+$ cells in the rat hippocampus after microwave radiation exposure (n = 5, the white arrows indicate $BrdU^+$&$Ki67^+$ cells, the magnified images shows $BrdU^+$&$Ki67^+$ cells in the R7d group). E, G and I: Results of immunofluorescence staining for BrdU and Nestin, for BrdU and DCX and for BrdU and NeuN in the DG region of the hippocampus in the control and radiation groups. F, H and J: Statistical analysis of the percentage of $BrdU^+$&$Nestin^+$, $BrdU^+$ & DCX^+ and $BrdU^+$ & $NeuN^+$ cells among $BrdU^+$ cells in the rat hippocampus after microwave radiation exposure (n = 5, the white arrows indicate $BrdU^+$ & $Nestin^+$, $BrdU^+$ & DCX^+ and $BrdU^+$ & $NeuN^+$ cells; the magnified images show $BrdU^+$ & $Nestin^+$, $BrdU^+$ & DCX^+, and $BrdU^+$ & $NeuN^+$ cells in the C28d and C6d groups). K: Quantification of *BDNF* mRNA expression. L: Western blot analysis of BDNF expression. M: Quantification of BDNF protein expression. (n = 5, for each sample, the experiment was conducted 3 times). Data are presented as mean ± SEM. Student's *t*-test was performed to compare the differences between two groups per time point. *, $p < 0.05$; **, $p < 0.01$. (C6h: control group, 6 h; R6h: radiation group, 6 h; C7d: control group, 7 d; R7d: radiation group, 7 d; C14d: control group, 14 d; R14d: radiation group, 14 d; C28d: control group, 28 d; R28d: radiation group, 28 d; scale bar = 50 μm).

microwave radiation, there was a significant decrease in the number of both $BrdU^+$ and $Ki67^+$ cells in the exposured groups compared to the control groups (n = 5, $p < 0.05$ or $p < 0.01$) (Fig. 4, C and D). This suggests an inhibition of the proliferation of newly born cells and also negates the possibility of microwave radiation inducing new cell generation via mitosis. Nestin is a marker for NSCs (NSCs), doublecortin (DCX) labels precursor cells and immature neurons, and neuronal nuclei (NeuN) is a marker for mature neurons. Therefore, we performed dual immunofluorescence staining for BrdU with Nestin, BrdU with DCX, and BrdU with NeuN to assess the differentiation stages of newly generated NSCs following microwave exposure (Fig. 4, E, G and I). At 6 h post-exposure, the proportion of $BrdU^+$ and $Nestin^+$ cells within the $BrdU^+$ population in the DG of the exposured group was significantly lower than that in the sham-operated group (n = 5, $p < 0.01$) (Fig. 4, F). At 6 h, 7 days, and 14 days post-exposure, the proportions of $BrdU^+$ and DCX^+ cells within the $BrdU^+$ population were significantly reduced (n = 5, $p < 0.05$ or $p < 0.01$) (Fig. 4, H), and at 14 days and 28 days post-exposure, the proportions of $BrdU^+$ and $NeuN^+$ cells within the $BrdU^+$ population were lower than those in the non-exposured group (n = 5, $p < 0.01$) (Fig. 4, J). These findings indicate that microwave exposure has a deleterious effect on the differentiation of NSCs.

BDNF is critically implicated in the regulation of synaptic plasticity and neural progenitor cell development. In this investigation, we quantified the alterations in BDNF gene and protein expression within the hippocampal region of rats subjected to microwave exposure by employing RT-qPCR and Western blot techniques. Our data reveal a substantial down-regulation in BDNF expression levels at both 7 and 28 days post-exposure to microwaves (n = 3, $p < 0.05$ or $p < 0.01$) (Fig. 4, K–M), implying that microwave exposure may induce synaptic plasticity disruptions and hinder neural stem cell proliferation and differentiation through the suppression of BDNF. Additionally, we examined the overall mRNA m^6A modification levels in the hippocampal region and found a significant decrease in modification levels at 6 h post-radiation (Fig. S1). These molecular changes are likely to contribute to the cognitive deficits and structural abnormalities that have been previously described.

3.5. In vitro co-culture model of primary hippocampal neurons and NSCs and influence of microwave radiation on both cell types

3.5.1. Exploration and optimization of co-culture medium formulation

In the context of co-culturing primary hippocampal neurons and NSCs, we embarked on a meticulous optimization of the culture medium formulation due to the intrinsic difficulties associated with their individual cultivation. As illustrated in Fig. 5, A, the diagram outlines the co-culture workflow for NSCs and primary hippocampal neurons. Fig. 5, B represents a schematic of the Transwell co-culture system, featuring an embedded co-culture chamber with an intervening semi-permeable polycarbonate membrane that impedes cellular passage while allowing the free diffusion of culture medium components.

At the outset, primary hippocampal neurons were maintained in their specialized medium within the upper chamber, while NSCs were cultured in a DMEM/F12-based medium of equivalent volume in the lower chamber. The impermeability of the polycarbonate membrane to cells, yet permissive to the diffusion of soluble factors, resulted in a homogeneous concentration of media components between the chambers. This initial approach, however, led to the detachment and suspension of hippocampal neurons, alongside the attachment and differentiation of NSCs, which precluded the maintenance of their stem-like spheroid morphology.

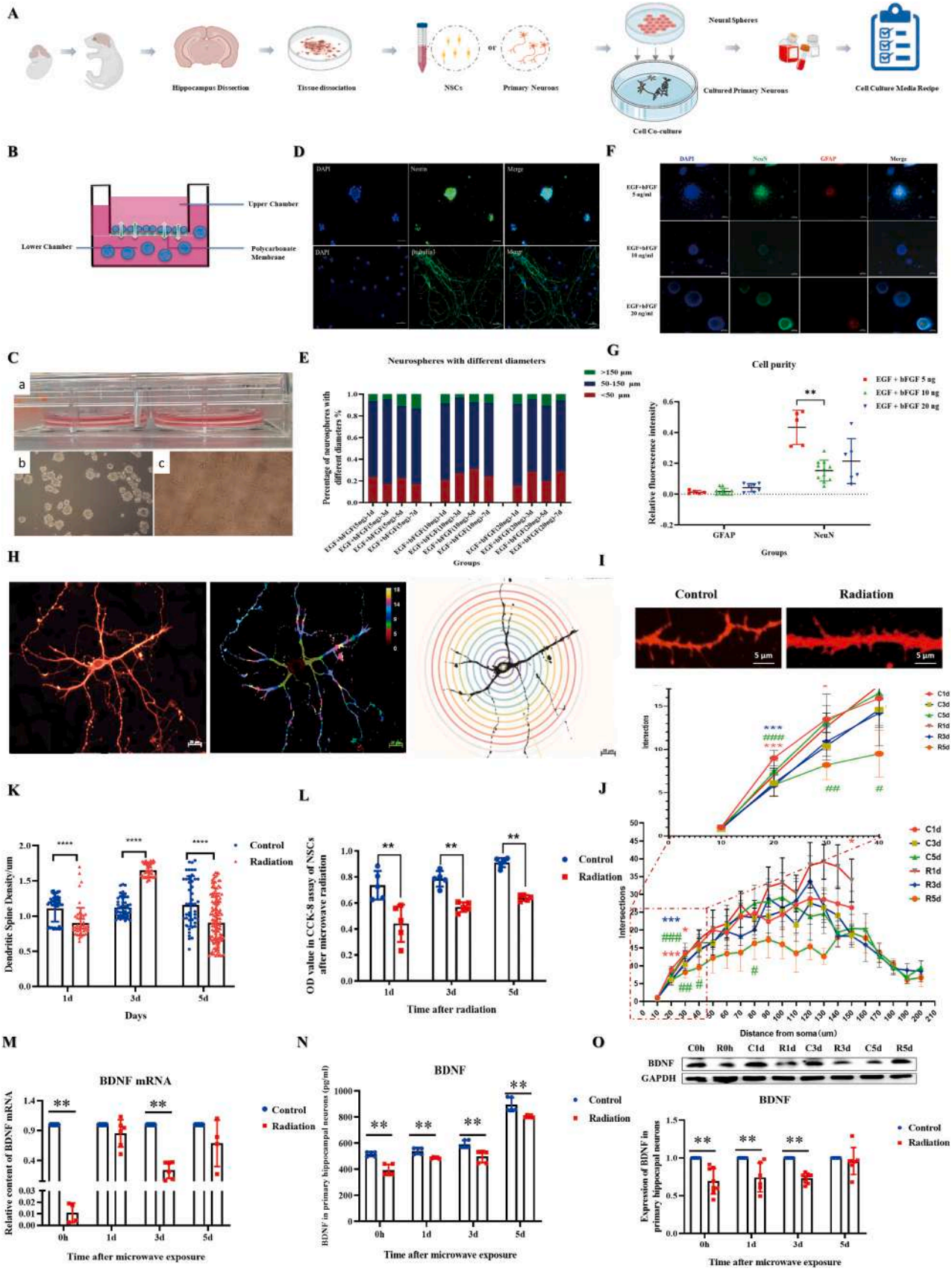
Further investigation, informed by an extensive literature review, suggested the viability of culturing NSCs in a Neurobasal-based medium, a shared component with primary hippocampal neuron culture medium (Wachs et al., 2003). Subsequent trials with Neurobasal supplemented with B27, Glutamax, and antibiotics resulted in rapid NSC adherence and differentiation, failing to preserve spheroid growth.

We then explored media formulations with altered Glutamax concentrations, including 0.5 % and Glutamax-free variations; however, these modifications did not ameliorate NSC differentiation. Recognizing the critical role of epidermal growth factor (EGF) and basic fibroblast growth factor (bFGF) in promoting NSC proliferation and stemness (Maric et al., 2003; Fortino et al., 2014), we supplemented the co-culture medium with both factors at 20 ng/ml. This addition fostered the formation of NSC spheroids while sustaining the growth of primary hippocampal neurons (Abe et al., 1991).

Accordingly, we established a provisional co-culture medium composition consisting of Neurobasal with B27, Glutamax, penicillin, EGF, and bFGF. To ensure the continuous proliferation of NSCs, it was essential to supplement EGF and bFGF bi-daily. This formulation has been determined to be the preliminary medium for co-culturing primary hippocampal neurons and NSCs (see in Section 2).

Following a 5-day cultivation in the designated co-culture medium, morphological assessments of NSCs and primary hippocampal neurons were performed using light microscopy. NSCs were observed to form tightly clustered, well-defined aggregates that resembled mulberries in shape and exhibited pronounced refractivity (Fig. 5, B (c)). Identification of NSCs was confirmed by staining with the specific marker Nestin. Concurrently, primary hippocampal neurons were visualized through immunofluorescent labeling with neuron-specific markers, revealing robust cell bodies and extensive neurite outgrowth, contributing to a dense network of neural fibers (Fig. 5, D).

In the optimization experiments for EGF + bFGF concentrations within the co-culture medium, the number of neurospheres within specified diameter ranges served as a metric for NSC proliferative capacity. Existing literature suggests that neurosphere growth reaches a rapid proliferation phase by day 3 post-passage and a plateau by day 6. It is also noted that neurospheres exceeding 150 μm in diameter may suffer from central necrosis due to inadequate nutrient diffusion. For this reason, neurospheres were categorized by diameters: < 50 μm, 50–150 μm, and > 150 μm, and were assessed under EGF + bFGF concentrations of 5 ng/ml, 10 ng/ml, and 20 ng/ml (Fig. 5, E). The 5 ng/ml group exhibited an increasing trend in the quantity of neurospheres larger than 150 μm, which did not stabilize as expected by day 7, indicating ongoing growth beyond the anticipated plateau. In contrast, the 10 ng/ml group displayed a stabilization in the proportion of neurospheres > 150 μm between days 5–7, aligning with the established proliferation patterns of NSCs. However, the 20 ng/ml group presented with irregular fluctuations in the distribution of neurosphere sizes during days 5–7, suggesting inconsistencies in NSC proliferation and sphere



(caption on next page)

Fig. 5. Microwave exposure attenuated synaptic plasticity in *ex vivo* cultured neurons and the proliferative capacity of NSCs. A: Schematic of the *in vitro* co-culture model of primary neurons and NSCs. B: Structural diagram of the Transwell chamber. C: Photographs of the Transwell co-culture system: (a) architecture of the Transwell chamber, (b) optical microscopy image of neurospheres, and (c) optical microscopy image of primary neurons. D: Immunofluorescence staining results for NSCs (Nestin, top) and primary neurons (Tubulin III, bottom) (scale bar = 50 μm). E: Quantification of neurosphere diameter distribution under various co-culture media over time. F and G: Evaluation of cellular purity and differentiation propensity in neurospheres using NeuN and GFAP immunofluorescence staining (scale bar = 50 μm, n ≥ 5). Data are mean ± SEM; one-way ANOVA was used for comparisons (**, $p < 0.01$). H: Images from Sholl analysis showing Tubulin III staining, Sholl Intersection Mask, and Overlay Sampling Shell with Intersection Points. I: Imaging results for dendritic spines within neuron segments. J: Line graph from Sholl analysis showing neuronal complexity, with the upper image b enlarged from the lower left dashed box (n = 10; *, R1d vs C1d, $p < 0.05$; ***, R1d vs C1d, $p < 0.01$; ***, R3d vs C3d, $p < 0.001$; #, R5d vs C5d, $p < 0.05$; ##, R5d vs C5d, $p < 0.01$; ###, R5d vs C5d, $p < 0.001$). K: Quantitative analysis of dendritic spine density following microwave exposure (15 neurons per group, and 3 dendritic segments on each neuron were chosen, n = 15). L: CCK-8 assay results on *ex vivo* NSCs after microwave radiation (n = 5). M: Effect of microwave radiation on *BDNF* mRNA expression (n = 5, each sample tested in quadruplicate). N: Impact of microwave radiation on BDNF protein expression—ELISA (n = 5, each sample tested in quadruplicate). O: Effects of microwave radiation on BDNF protein expression—Western blot (n = 5, each sample tested in five replicates). Data are mean ± SEM; Student's *t*-test for two-group comparisons (*, $p < 0.05$; **, $p < 0.01$; ***, $p < 0.001$). (C0h: control group, 0 h; R0h: radiation group, 0 h; C1d: control group, 1 d; R1d: radiation group, 1 d; C3d: control group, 3 d; R3d: radiation group, 3 d; C5d: control group, 5 d; R5d: radiation group, 5 d; scale bar = 50 μm).

formation.

Further analysis through immunofluorescence staining provided semi-quantitative insights into the differentiation propensities of NSCs within neurospheres towards mature neurons and astrocytes (Fig. 5G). Neurospheres in the EGF + bFGF (5 ng/ml) condition showed a richer expression of NeuN, indicative of a greater number of mature neurons, and a pronounced emergence of neuritic processes surrounding the spheres. Quantitatively, the total fluorescence intensity was significantly higher than in the 10 ng/ml condition ($p < 0.05$), pointing to a differentiation bias towards neuronal lineage. GFAP expression, indicative of astrocytic differentiation, did not differ significantly across the tested conditions.

Based on these comprehensive analyses, EGF + bFGF at a concentration of 10 ng/ml was established as the optimal formulation for the co-culture medium of NSCs and primary hippocampal neurons.

3.6. The effects of microwave radiation on synaptic plasticity of in vitro neurons and proliferative capacity of NSCs

Subsequent evaluations of microwave exposure's impact on *ex vivo* neurons were meticulously performed according to the developmental patterns of dendritic spines and synaptic plasticity in *ex vivo* neurons (Beaudoin et al., 2012), utilizing immunofluorescent staining in conjunction with detailed morphometric analysis. Sholl analysis was employed to appraise neuronal complexity, while dendritic spine density was rigorously quantified (Fig. 4, H and I). Statistical analysis indicated that at 1, 3, and 5 days post microwave radiation, there was a significant decrement in the number of neuronal branches proximal to 20 μm from the cell soma compared with corresponding time-matched controls (n = 10, $p < 0.001$). Furthermore, at distances of 40 μm and 80 μm from the soma, a significant reduction in neuronal branching was observed after 5 days of microwave exposure relative to controls (n = 10, $p < 0.05$ or $p < 0.01$) (Fig. 4, J). Additionally, the exposure group exhibited a significant reduction in dendritic spine density at 1 and 5 days post-exposure when compared to the control group (for each experimental group and at each designated time point, a sample of 15 neurons was selected, and from each neuron, three dendrites were chosen for dendritic spine analysis, n = 45, $p < 0.001$). Intriguingly, at 3 days post-exposure, there was a significant increase in dendritic spine density in the exposure group versus the control (n = 45, $p < 0.001$) (Fig. 4, K). These data imply that microwave exposure can precipitate synaptic development aberrations and disrupt dendritic spine plasticity at the level of dissociated neurons.

With respect to the influence of microwave exposure on NSCs, the Cell Counting Kit-8 (CCK-8) assay was implemented for analytical investigation. The assay outcomes demonstrated a significant reduction in the optical density of NSCs within the exposure cohort when compared to the control group at 1, 3, and 5 days subsequent to exposure (n = 5, $p < 0.01$) (Fig. 4, L), signifying a considerable inhibitory effect on neural stem cell proliferative capabilities post-exposure.

3.7. The effects of microwave radiation on BDNF expression of in vitro neurons

In alignment with *in vivo* experimental paradigms, the gene and protein expression levels of BDNF were assiduously assessed in isolated neuronal cultures. On the transcriptional axis, exposure to microwave radiation elicited a marked attenuation in the expression of *BDNF* mRNA at time points immediately post-exposure (0 h) and at 3 days in comparison to the non-exposed control cohort (n = 4, $p < 0.01$) (Fig. 4, M). At the proteomic level, quantitative analysis via Enzyme-Linked Immunosorbent Assay (ELISA) revealed that BDNF protein expression was consistently and significantly diminished across all post-exposure time intervals under scrutiny, when juxtaposed with control values (n = 5, $p < 0.01$) (Fig. 4, N). These observations were further substantiated by Western blot analyses, which demonstrated a substantial down-regulation in BDNF protein expression at 0 h, 1 day, and 3 days following microwave exposure, as compared with the control specimens (n = 5, $p < 0.01$) (Fig. 4, O). The overall mRNA m^6A modification levels were significantly down-regulated immediately after radiation (n = 3, $p < 0.01$) (Fig. S2). The m^6A modification-related genes showed dysregulated expression as well (n = 3, $p < 0.05$ or $p < 0.01$) (Fig. S3). Such findings exhibit congruence with the molecular alterations documented within the *in vivo* research context.

3.8. Comprehensive analysis of the transcriptome-wide m^6A methylome in radiated neurons by MeRIP-seq

Given the bridging role of epigenetics between environmental factors and phenotypes, coupled with the significant impact of microwave exposure on *BDNF* mRNA and protein expression observed in our previous studies, we further investigated the epigenetic transcriptional mechanisms as a starting point. Since BDNF is primarily secreted by neurons in the co-culture system we established, we focused on primary neurons exposed to microwaves at 0 h, when significant differences in BDNF protein and gene expression have already emerged. MeRIP-seq analysis was conducted on three cases of microwave-exposed primary neurons and control group neurons. Fig. 6, A depicts the experimental workflow of MeRIP-seq sequencing analysis. The sequence motifs displayed are the top three enriched m^6A motifs, with "GGAC" sequence highlighted by a red box (Fig. 6, B). Further investigation was conducted to examine the distribution of m^6A peaks in the control and radiation groups. As shown in Fig. 6, C and D, the distribution of m^6A signals around mRNA was similar in both groups. The m^6A peaks in mRNA were primarily enriched in the coding sequences near the stop codons. Compared to the control group, the radiation group exhibited 1119 significantly upregulated peaks corresponding to 1019 transcriptomes of genes (Fold change ≥ 2 and $p < 0.05$), and 985 significantly down-regulated peaks corresponding to 907 transcriptomes of genes (Fold change ≥ 2 and $p < 0.05$). Table 1 presents the top 20 peaks with the highest changes. By analyzing the distribution of m^6A peaks in each

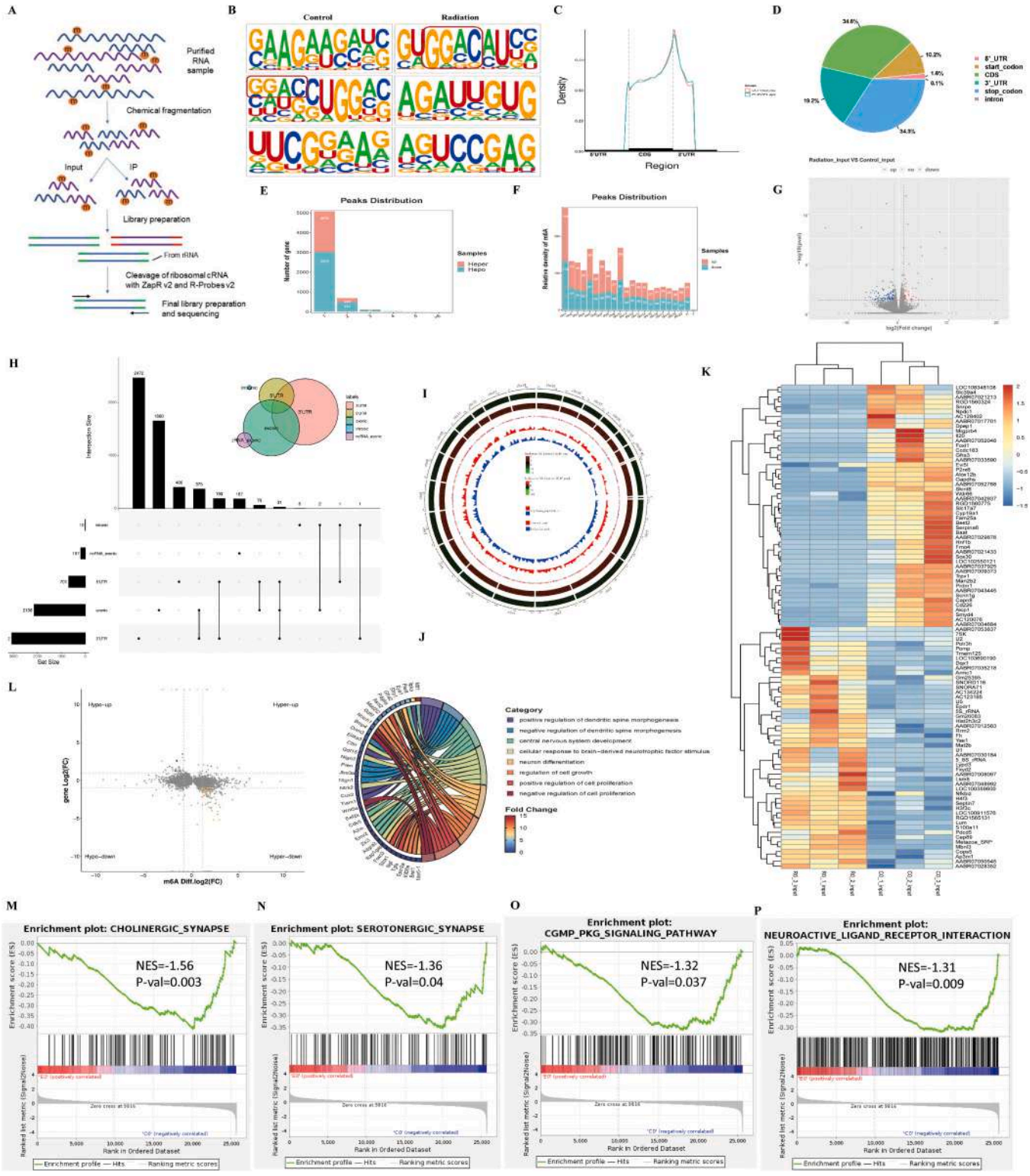


Fig. 6. Comprehensive analysis of the transcriptome-wide m^6A methylome in radiated neurons by MeRIP-seq. A: The experimental workflow of MeRIP-seq. B: The sequence logo showed the top three m^6A motifs. C: The distribution of m^6A peaks in control and radiated neurons. D: Pie charts showing the distribution of differently methylated m^6A peak. E: The distribution of methylated m^6A peaks mRNA. F: The distribution of methylated m^6A peaks in chromosomes. G: Volcano plot showing the top differentially expressed genes in radiation groups vs control. H: Exact distribution pattern of significantly changed peaks post-radiation. I: The distribution pattern of m^6A peaks and mRNA in different chromosomes. J: Chord diagram of significantly enriched genes organized for GO terms relevant to this study. K: A heatmap displaying the top 100 differentially expressed genes with the smallest p-values was generated in radiation groups vs control. L: Four-quadrant plots showing the distribution of genes with significant changes in both the m^6A modification and RNA levels. M-P: GSEA enrichment of genes with significant changes in both the m^6A modification and RNA levels.

Table 1
Top 20 differently methylated m^6A peaks in Radiation groups vs Control.

Gene ID	Gene Name	Chromosome	Peak_Length	Log2FC	pvalue	Annotation
ENSRNOG00000026672	*MGC94199*	chr5	568	− 18.79	NA	UTR3
ENSRNOG00000046867	*Zfp260*	chr1	451	− 9.65	0.00	exonic
ENSRNOG00000009617	*Exoc7*	chr10	4430	9.38	0.00	exonic
ENSRNOG00000046867	*Zfp260*	chr1	126	− 8.29	0.00	exonic
ENSRNOG00000010589	*Zfp622*	chr2	1244	7.43	0.00	UTR3
ENSRNOG00000018291	*Vkorc1l1*	chr8	3827	− 7.31	0.00	exonic
ENSRNOG00000060047	*LOC108348083*	chr1	351	6.09	0.00	UTR3
ENSRNOG00000055330	*AABR07039234*	X	326	6.06	0.00	ncRNA_exonic
ENSRNOG00000002548	*Tnn*	chr13	326	− 6.05	0.00	intronic
ENSRNOG00000046211	*Fbxw4*	chr1	14,820	5.80	0.00	exonic
ENSRNOG00000013602	*Usp48*	chr5	6046	5.72	0.00	exonic
ENSRNOG00000001770	*Ehhadh*	chr11	251	5.58	0.00	UTR3
ENSRNOG00000057696	*Sbk1*	chr1	351	5.53	0.00	UTR5
ENSRNOG00000020857	*Ppfia1*	chr1	3438	− 5.24	0.00	UTR3
ENSRNOG00000024889	*Snip1*	chr5	4740	− 5.20	0.00	exonic
ENSRNOG00000049236	*Myh9l1*	chr7	979	5.13	0.00	exonic
ENSRNOG00000001738	*Eif4g1*	chr11	176	5.07	NA	exonic
ENSRNOG00000045877	*AC098547*	chr20	1456	− 5.02	0.00	ncRNA_exonic
ENSRNOG00000052389	*AABR07031489*	chr18	126	− 4.75	0.00	ncRNA_exonic

3'UTR, 3′ untranslated region; 5′UTR, 5′ untranslated region; ncRNA, non-coding RNA; exon, expressed region.

mRNA, we found that most mRNAs contained one peak (Fig. 6, E). All altered m^6A peaks were located on human chromosomes. Disrupted m^6A peaks were observed on all chromosomes, particularly on chr1, chr2, chr16, chr17, and chr19 (Fig. 6, F). Many peaks with significant changes spanned multiple gene structures, with 375 peaks distributed in the exonic and 3′ UTR regions, 193 peaks in the 5′ UTR, exonic, and 3′ UTR regions, and 70 peaks in the 5′ UTR and exonic regions (Fig. 6, H). Combining the above results, we plotted the distribution of differential transcripts, differential peaks, and the corresponding chromosomes of each group's m^6A peaks (Fig. 6, I). Additionally, we depicted a chord diagram showing the genes enriched by the significant differentially expressed peaks of interest (Fig. 6, J). To investigate the biological significance of m^6A modification in microwave radiation-induced neuronal functional abnormalities, we performed GO term and KEGG pathway analyses on differentially methylated genes. The bar charts of GO enrichment analysis results displayed the distribution of differentially expressed genes in enriched GO terms in biological processes (TOP25), cellular components (TOP15), and molecular functions (TOP10) (Fig. S3, A and B). KEGG pathway analysis revealed significant associations between genes exhibiting differential m^6A peaks after microwave radiation and cancer, the PI3K-Akt signaling pathway, and the MAPK signaling pathway (Fig. S3, C).

Transcriptome profiles of the two sample groups were examined using RNA-Seq (MeRIP-Seq input libraries). Compared to the control group, the radiation group displayed upregulation of 42 genes and down-regulation of 111 genes (Fig. 6, G). The heatmap depicted the top 100 genes with the smallest p-values (Fig. 6, K). Subsequently, a combined analysis of MeRIP-seq and RNA-seq data classified all differentially methylated m^6A peaks with differential RNA levels (216) into four groups. The results revealed that 150 highly methylated m^6A peaks in RNA were significantly upregulated (10; hyper-up) or down-regulated (140; hyper-down), while 66 lowly methylated m^6A peaks peaked in significantly upregulated RNA (40; hypo-up) or down-regulated RNA (26; hypo-down) (Fig. 6, L). GO and KEGG pathway analyses were conducted on the 216 differentially methylated m^6A peaks and synchronously differentially expressed genes. GO analysis indicated that these genes were mainly enriched in signal transduction (BP), membrane (CC), and protein binding (MF) (Fig. S4, A and B). KEGG pathway analysis revealed enrichment of these genes in signaling pathways such as Neuroactive ligand-receptor interaction, Signaling pathways regulating pluripotency of stem cells, and Proteoglycans in cancer (Fig. S4, C). In contrast, GSEA enrichment analysis of genes with significant changes in m^6A modification and RNA levels suggested that these genes were enriched in CHOLINERGIC_SYNAPSE, SEROTONERGIC_SYNAPSE, CGMP_PKG_SIGNALING_PATHWAY, and NEUROACTIVE_LIGAND_RECEPTOR_INTERACTION signaling pathways (Fig. 6, M–P).

3.9. HNRNPA2B1 down-regulates BDNF expression through feed forward regulation via m^6A-dependent destabilization of TrkB mRNA after microwave radiation

In joint analysis, we observed a significant decrease in m^6A peaks and gene expression levels of the BDNF receptor *TrkB* (*NTRK2*) (Fig. 7, A, Fig. S5). Biological experiments confirmed a significant reduction in mRNA and protein expression of TrkB after microwave radiation exposure (Fig. 7, B–D), suggesting a potential role of the aforementioned m^6A modification site in maintaining mRNA stability. To further elucidate the involvement of specific methylation-related proteins (writers/erasers/readers) in this process, we employed a probe-based RNA pull-down experiment targeting *TrkB* (Fig. 7, E–F), followed by mass spectrometry identification of proteins interacting with *TrkB* RNA (see Fig. S6 for mass spectrometry quality control results and the bioinformatics analysis results of identified proteins). HNRNPA2B1 was found to interact with *TrkB* mRNA. Subsequently, we examined the gene and protein expression of HNRNPA2B1 and found a significant down-regulation following microwave radiation exposure (Fig. 7, G and H). These results suggest that HNRNPA2B1 is down-regulated and regulates BDNF through a *TrkB* mRNA m^6A-dependent mechanism. Additionally, we predicted potential m^6A modification sites in *TrkB* using the SRAMP database (http://www.cuilab.cn/sramp) and identified five highly credible sites, including 1860: AGACU/PPBPP, 2412: GGACU/PPMPP, 2703: GAACU/PPIPP, 2752: GGACU/PPPPH, 3087: GAACU/IIIII, and plotted their RNA secondary structures (Fig. 7, I–K), laying the foundation for future intervention experiments.

4. Discussion

A multitude of compelling evidence supports the assertion that electromagnetic radiation has the potential to serve as a stressor, thereby exerting discernible impacts on organisms (McCredden et al., 2022; Association, 2012). In the nervous system, these effects are primarily manifested as learning and memory impairments (Hao et al., 2023; Jiang et al., 2024). The hippocampus, an important brain region for learning and memory, is particularly vulnerable to microwave radiation-induced cognitive impairments, with the DG region being prominently affected (Wang et al., 2013; Zhi et al., 2018). The DG region is also a major site for adult neurogenesis, where newly generated neurons integrate into existing learning and memory circuits within

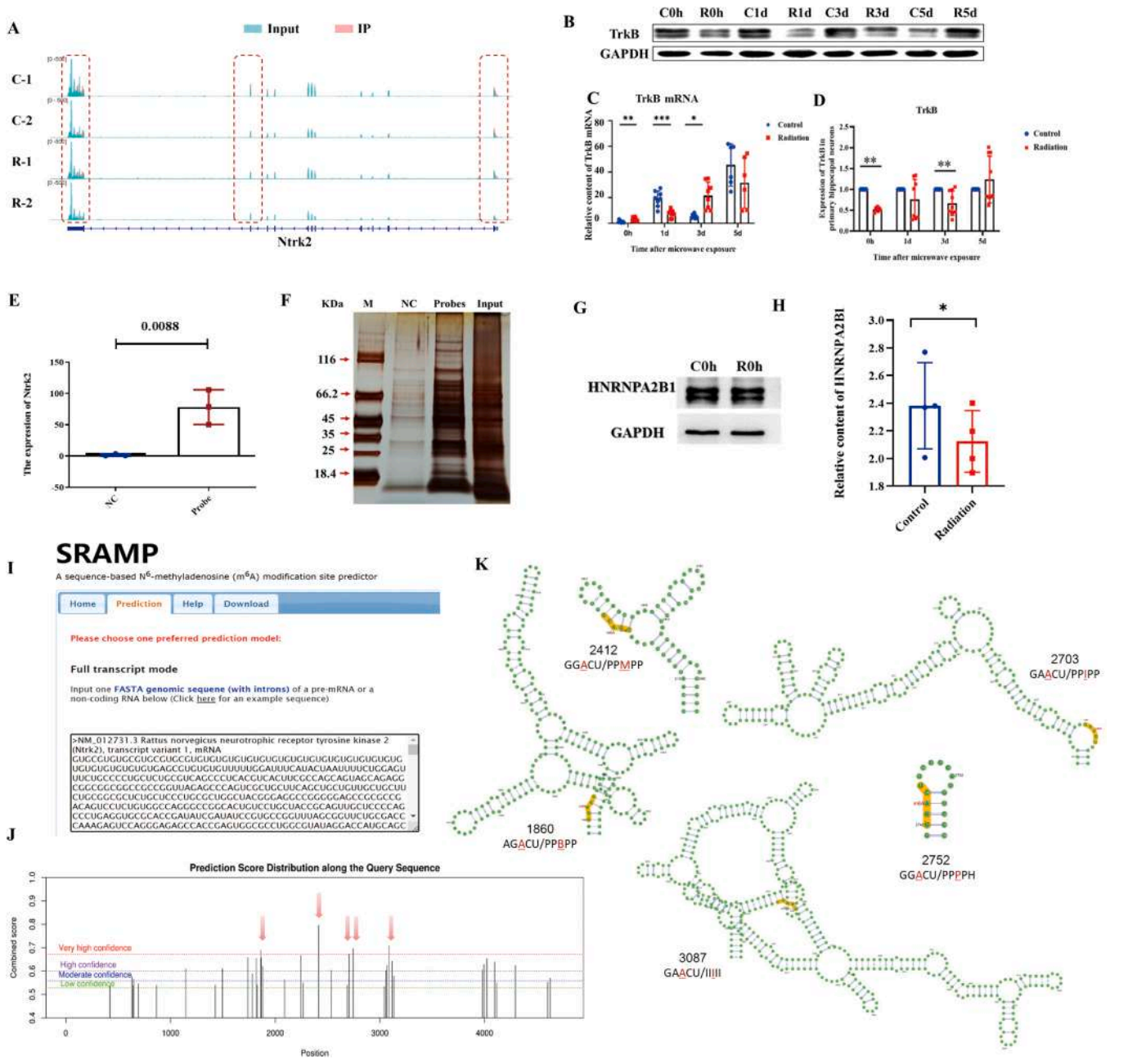


Fig. 7. HNRNPA2B1 down-regulates BDNF expression through feed forward regulation via m^6A-dependent destabilization of *TrkB* mRNA after microwave radiation. A: m^6A signal in exposure group were decreased at specific positions of *TrkB* (C-1 and C-2 represent two biological replicates of the sham radiation group; R-1 and R-2 represent two biological replicates of the radiation group, m^6A modification sites with differential expression are indicated by red dashed circles). B: Western blot analysis of TrkB protein expression under the influence of microwave radiation. C: Impact of microwave radiation on *TrkB* mRNA expression (n = 6, the experiment was performed in quadruplicate for each sample, *, $p < 0.05$; **, $p < 0.01$). D: Quantitative analysis of TrkB protein expression by Western blot (n = 5, the experiment was conducted 6 times for each sample, *, $p < 0.05$; **, $p < 0.01$). E: q-PCR quantification of *TrkB* content in *TrkB* RNA pull-down assay products. F: Silver staining of *TrkB* RNA pull-down assay. G–H: Effects of microwave radiation on HNRNPA2B1 protein expression-Western blot (n = 3, for each sample, the experiment was conducted 4 times, *, $p < 0.05$; **, $p < 0.01$). I–J: Prediction results of *TrkB/NTRK2* mRNA in SRAMP website show the potential site of m^6A modification. The red arrow points sites with very high confidence. K: The secondary structure of potential site of m^6A modification on *TrkB/NTRK2* mRNA predicted in SRAMP website.

three weeks (Gonçalves et al., 2016; Bond et al., 2015). Therefore, we propose that the impact of microwave radiation on synaptic plasticity in the DG region can be attributed to alterations in the synaptic connections and plasticity of both mature neurons and newly generated neurons derived from stem cells. To investigate this, we first established a rat model of microwave radiation-induced cognitive impairments and excluded the influence of thermal effects. In this model, we first controlled the temperature increase caused by radiation to within 1 °C, which is considered unlikely to cause adverse effects on the function of the nervous system structure (Owen et al., 2019; Ouares et al., 2019; Galvan et al., 2017; Yarmolenko et al., 2011). Then we specifically elucidated the effects of microwave radiation on synaptic plasticity in the DG region of the rat hippocampus and on adult neurogenesis. The results confirmed that microwave radiation at this dosage significantly impairs synaptic structural plasticity in DG neurons, as evidenced by suppressed mossy fiber sprouting and reduced length and thickness of

postsynaptic densities. Additionally, microwave radiation inhibited the proliferation, migration, and differentiation of NSCs in the DG region, showing consistency with the developmental pattern of NSCs (Vadodaria and Sebastian, 2014; Abbott and Nigussie, 2020). These findings collectively indicate that microwave radiation impairs learning and memory functions in rats by affecting the synaptic plasticity involving both mature neurons and NSCs in the DG region.

At the molecular level, based on previous research, BDNF has been identified as a key player in synaptic plasticity and neural stem cell development, and its expression is disrupted following microwave radiation exposure (Wang et al., 2006; Zhang et al., 2006; Urnukhsaikhan et al., 2006). However, how does microwave radiation, as an external environmental stimulus, affect protein expression in the body? Epigenetic modifications, serving as a pivotal linkage connecting environmental influences with organismic responses, constitute a logical and justifiable entry point for further scientific inquiry (Cavalli and Heard, 2006; Tammen et al., 2006). To gain a deeper understanding of the underlying molecular mechanisms, we initially established a co-culture model involving primary hippocampal neurons and NSCs. This approach allows us to explore the interactions and interdependencies between these two cell types in a controlled environment. This model was constructed utilizing transwell chambers, which facilitate the unrestricted diffusion of soluble molecules between the upper and lower compartments while effectively impeding cell migration through a semi-permeable membrane. This innovative setup preserves the physiological characteristics of both primary hippocampal neurons and NSCs, thereby enabling reciprocal interactions mediated by the secretion of cellular factors. Furthermore, it permits comprehensive morphological and molecular analysis of both cell types in their respective chambers, providing insights into their dynamic interplay under controlled conditions. Upon exposure to microwave radiation, a notable suppression of dendritic growth and dendritic spine development was observed in primary hippocampal neurons, along with a significant reduction in the proliferative activity of NSCs. Additionally, both protein and gene expression of BDNF were down-regulated, indicating a modulation of neurotrophic support mechanisms. These findings implicate that the adverse effects of microwave radiation on neurons and NSCs *in vitro* mirror those observed *in vivo*, rendering this model a viable surrogate for further elucidating the underlying molecular mechanisms involved in these processes.

In terms of the m^6A modification, MeRIP-seq sequencing analysis has initially disclosed comprehensive modifications in the overall patterns of mRNA m^6A modification within neurons subsequent to exposure to microwave radiation. This revelation suggests profound disparities in the transcriptional profiles of genes exhibiting sensitivity to BDNF stimulation, alongside genes integral to the intricate processes of synaptic plasticity regulation and NSCs development. These deductions, formulated on the basis of a rigorous enrichment analysis, provide an enhanced comprehension of the intricate transcriptional consequences elicited by microwave radiation at the epigenetic level. Despite the absence of differential m^6A modification peaks within the *BDNF* gene, our study revealed significant alterations in m^6A peak distribution specifically within the *TrkB* receptor. Specifically, exposure to microwave radiation elicited a noteworthy down-regulation of m^6A modification on *TrkB*, which aligned with the diminution of both mRNA and protein expression levels observed in biological experiments. Furthermore, the pattern of changes in BDNF expression following radiation exposure exhibited parallelism with that observed in TrkB, suggesting potential interconnectedness between these molecules in response to radiation. Additionally, notable differences in m^6A peak patterns and gene expression associated with the PI3K-Akt and MAPK signaling pathways were evident between the two experimental groups, underscoring the complex neurobiological effects associated with microwave radiation exposure. Studies have shown that TrkB, activated by its ligand BDNF, acts as an effective regulator of development and adult plasticity, playing a role in neural pruning and branching events during neurodevelopment, as well as in learning and memory (Vantini and Skaper, 2006; Minichiello, 2006). The PI3K-Akt signaling pathway and MAPK signaling pathway are also associated with local TrkB-related developmental events and synaptic regulation (Atwal et al., 2000; Cheng et al., 2011; Reichardt, 2006; De Vincenti et al., 2019; Yoshii and Constantine-Paton, 2010). Furthermore, locally synthesized BDNF/TrkB signaling has been demonstrated to exert localised autocrine effects within discrete dendritic spines, suggesting intricate, compartment-specific regulatory mechanisms (Harward et al., 2016a): BDNF activation of TrkB in the synaptic cleft triggers calcium release from the endoplasmic reticulum, followed by calcium-dependent enhancement of BDNF release from the postsynaptic site via NMDARs and CaMKII. This process can be summarized as a feed-forward loop of TrkB signaling (Harward et al., 2016a). In the present investigation, it is hypothesized that the down-regulation of TrkB protein expression might potentially trigger a reduction in the expression and secretion of BDNF via a feed-forward loop mechanism. Consequently, this down-regulation could mediate the suppression of dendritic growth and dendritic spine formation within neurons, as well as perturbations in the developmental processes of NSCs. These effects are presumed to occur as a consequence of exposure to microwave radiation (Anerillas et al., 2016; Wang et al., 2016; Harward et al., 2016b). The down-regulation of m^6A modification on TrkB protein indicates its potential significance in regulating mRNA stability. Utilizing mass spectrometry analysis to interrogate the proteome of proteins interacting with *TrkB* mRNA, we serendipitously discovered the interaction between HNRNPA2B1 and *TrkB* mRNA. HNRNPA2B1 functions as an m^6A reader, selectively binding to nascent RNA and exercising intricate control over a diverse array of RNA metabolic processes. Specifically, it identifies m^6A modifications within specific genes, ultimately contributing to the enhancement of their stability (Jiang et al., 2021b). In the present study, we observed a down-regulation of HNRNPA2B1 protein expression accompanied by reduced levels of m^6A modifications on the *TrkB* mRNA following exposure to microwave radiation. Based on these observations, we hypothesize that the interaction between HNRNPA2B1 and the m^6A sites within the *TrkB* mRNA is also attenuated. This reduced binding likely results in diminished stability of the *TrkB* mRNA, leading to its degradation and ultimately a decrease in TrkB protein expression following microwave radiation exposure. This dysregulation of TrkB, which is modulated by feed-forward loop signaling, may contribute to insufficient expression of BDNF and thereby abnormal synaptic plasticity in the hippocampal DG region, ultimately leading to cognitive impairment in rats. Certainly, the aforementioned conclusions are reasonable inferences drawn solely from the results of the current study and the mechanisms reported in the existing authoritative literature. Further experimental research is required in the future to provide more definitive evidence. Additionally, our bioinformatics analysis successfully identified five highly credible candidate m^6A modification sites within the *TrkB* gene, providing potential targets for future interventional and validation studies.

5. Conclusion

In summary, our comprehensive study offers profound insights into the intricate mechanisms underlying the induction of cognitive impairments by microwave radiation through dysregulation of m^6A epigenetic modifications. We have established that HNRNPA2B1 maintains the stability of *TrkB* mRNA in a manner that relies on the presence of *TrkB* m^6A modifications. However, upon exposure to microwave radiation, we observed a notable decrease in both HNRNPA2B1 levels and *TrkB* m^6A modifications, leading to a subsequent reduction in TrkB expression. Within NSCs, this reduction in TrkB expression results in decreased uptake of BDNF, which impairs cellular proliferation and differentiation processes. Furthermore, within the synaptic structures of neurons, a feed-forward loop mechanism ensues, causing decreased BDNF secretion. This, in turn, inhibits dendritic growth in mature

neurons and leads to aberrant synaptic plasticity. Collectively, the combined effects of these cellular alterations contribute to the observed cognitive impairments in rats following microwave radiation exposure. Future interventional strategies and validation studies aimed at targeting the predicted *TrkB* m^6A modification sites hold promise as potential therapeutic and protective targets for addressing cognitive impairments linked to microwave radiation exposure. This investigation represents a significant advancement in our understanding of these complexities and offers crucial insights for the development of novel interventional strategies.

Environmental implications

This study highlights significant environmental implications of microwave radiation on cognitive function, raising concerns about long-term neurocognitive impacts due to its ubiquitous exposure. It emphasizes the role of epigenetic mechanisms, particularly HNRNPA2B1's regulation of BDNF expression through m^6A-dependent destabilization of *TrkB* mRNA, providing novel insights into microwave-induced cognitive impairments. Identifying *TrkB* m^6A modification as a protective target offers new strategies for mitigating these effects. The findings underscore the need for further research into microwave radiation's environmental health effects and the importance of epigenetic considerations in protecting human health in our increasingly electromagnetic environment.

Funding statement

Support for this research was provided by National Natural Science Foundation of China, Grant no.: 31800701.

CRediT authorship contribution statement

Zhao Xuelong: Data curation. **Yang Zhenqi:** Methodology. **Dong Ji:** Data curation. **Yao Binwei:** Data curation. **Wang Lifeng:** Writing – review & editing, Conceptualization. **Lin Zhongwu:** Writing – review & editing. **Zhi Weijia:** Writing – original draft, Data curation, Conceptualization. **Hu Xiangjun:** Writing – review & editing. **Tang Jiale:** Writing – original draft, Data curation. **Qiao Simo:** Data curation. **Ma Lizhen:** Data curation. **Zhang Mingzhao:** Data curation. **Zou Yong:** Data curation.

Declaration of Competing Interest

The authors declare that they have no known competing financial interests or personal relationships that could have appeared to influence the work reported in this paper.

Acknowledgements

W.Z. and J.T. contributed equally to this work.

The authors would like to thank Ying Li, Fan Xv, Yuan Yuan and Yinxia Wang (Beijing Institute of Radiation Medicine) for animal and cell culture.

Appendix A. Supporting information

Supplementary data associated with this article can be found in the online version at doi:10.1016/j.ecoenv.2025.117907.

Data availability

Data will be made available on request.

References

Abbott, L.C., Nigussie, F., 2020. Adult Neurogenesis in the Mammalian Dentate Gyrus. John Wiley & Sons, Ltd.

Abe, K., Takayanagi, M., Saito, H., 1991. Basic fibroblast growth factor and epidermal growth factor promote survival of primary cultured cerebellar neurons from neonatal rats. Jpn. J. Pharmacol. 56, 113–116.

Abe, Y., Erchinger, V.J., Ousdal, O.T., Oltedal, L., Tanaka, K.F., Takamiya, A., 2024. Neurobiological mechanisms of electroconvulsive therapy for depression: insights into hippocampal volumetric increases from clinical and preclinical studies. J. Neurochem.

Afhami, M., Behnam-Rassouli, M., Gorji, A., Karima, S., Shahpasand, K., 2023. Isolation and culture of neural stem/progenitor cells from the hippocampal dentate gyrus of young adult and aged rats. Bio-Protocol 13.

Aimone, J.B., Wiles, J., Gage, F.H., 2006. Potential role for adult neurogenesis in the encoding of time in new memories. Nat. Neurosci. 9, 723–727.

Alarcón, C.R., Goodarzi, H., Lee, H., Liu, X., Tavazoie, S., Tavazoie, S.F., 2015. HNRNPA2B1 is a mediator of m(6)A-dependent nuclear RNA processing events. Cell. S0092867415010247.

Anerillas, C., Herman, A.B., Munk, R., Garrido, A., Lam, K.-W.G., Payea, M.J., Rossi, M., Tsitsipatis, D., Martindale, J.L., Piao, Y., Mazan-Mamczarz, K., Fan, J., Cui, C.-Y., De, S., Abdelmohsen, K., de Cabo, R., Gorospe, M., 2016. A BDNF-TrkB autocrine loop enhances senescent cell viability. Nat. Commun. 13, 6228.

Association, A.M., 2012. Guideline of the Austrian Medical Association for the diagnosis and treatment of EMF-related health problems and illnesses (EMF syndrome). In: Consensus paper of the Austrian Medical Association's EMF Working Group (AG-EMF). Meeting of environmental medicine officers Serious health issue of the Regional Medical Association's and the Austrian Medical Association, Vienna, Austria.

Atwal, J.K., Massie, B., Miller, F.D., Kaplan, D.R., 2000. The TrkB-Shc site signals neuronal survival and local axon growth via MEK and PI3-kinase. Neuron 27, 265–277.

Beaudoin, G.M., Lee, I.I.I.S.-H., Singh, D., Yuan, Y., Ng, Y.-G., Reichardt, L.F., Arikkath, J., 2012. Culturing pyramidal neurons from the early postnatal mouse hippocampus and cortex. Nat. Protoc. 7, 1741–1754.

Binley, K.E., Ng, W.S., Tribble, J.R., Song, B., Morgan, J.E., 2006. Sholl analysis: a quantitative comparison of semi-automated methods. J. Neurosci. Methods 225, 65–70.

Bond, A.M., Ming, G.-l, Song, H., 2015. Adult mammalian neural stem cells and neurogenesis: five decades later. Cell Stem Cell 17, 385–395.

Burgio, E., Migliore, L., 2015. Towards a systemic paradigm in carcinogenesis: linking epigenetics and genetics. Mol. Biol. Rep. 42, 777–790.

Carpenter, D.O., 2013. Human disease resulting from exposure to electromagnetic fields. Rev. Environ. Health 28, 159–172.

Cavalli, G., Heard, E., 2006. Advances in epigenetics link genetics to the environment and disease. Nature 571, 489–499.

Chen, Y.-h, Zhang, R.-g, Xue, F., Wang, H.-n, Chen, Y.-c, Hu, G.-t, Peng, Y., Peng, Z.-w, Tan, Q.-r, 2015. Quetiapine and repetitive transcranial magnetic stimulation ameliorate depression-like behaviors and up-regulate the proliferation of hippocampal-derived neural stem cells in a rat model of depression: the involvement of the BDNF/ERK signal pathway. Pharmacol. Biochem. Behav. 136, 39–46.

Cheng, P.-L., Song, A.-H., Wong, Y.-H., Wang, S., Zhang, X., Poo, M.-M., 2011. Self-amplifying autocrine actions of BDNF in axon development. Proc. Natl. Acad. Sci. 108, 18430–18435.

Cui, M., Ge, H., Zhao, H., Zou, Y., Chen, Y., Feng, H., 2017. Electromagnetic fields for the regulation of neural stem cells. Stem Cells Int. 2017, 9898439.

De Vincenti, A.P., Ríos, A.S., Paratcha, G., Ledda, F., 2019. Mechanisms that modulate and diversify BDNF functions: implications for hippocampal synaptic plasticity. Front. Cell. Neurosci. 13, 135.

Ferreira, T., Ou, Y., Li, S., Giniger, E., van Meyel, D.J., 2014. Dendrite architecture organized by transcriptional control of the F-actin nucleator spire. Development 141, 650–660.

Fortino, V.R., Chen, R.S., Pelaez, D., Cheung, H.S., 2014. Neurogenesis of neural crest-derived periodontal ligament stem cells by EGF and bFGF. J. Cell. Physiol. 229, 479–488.

Gage, F.H., Coates, P.W., Palmer, T.D., Kuhn, H.G., Fisher, L.J., Suhonen, J.O., Peterson, D.A., Suhr, S.T., Ray, J., 1995. Survival and differentiation of adult neuronal progenitor cells transplanted to the adult brain. Proc. Natl. Acad. Sci. 92, 11879–11883.

Galvan, A., Stauffer, W.R., Acker, L., El-Shamayleh, Y., Inoue, K.-i., Ohayon, S., Schmid, M.C., 2017. Nonhuman primate optogenetics: recent advances and future directions. J. Neurosci. 37, 10894–10903.

Gonçalves, J.T., Schafer, S.T., Gage, F.H., 2016. Adult neurogenesis in the hippocampus: from stem cells to behavior. Cell 167, 897–914.

Hao, Y., Liu, W., Liu, Y., Liu, Y., Xu, Z., Ye, Y., Zhou, H., Deng, H., Zuo, H., Yang, H., 2023. Effects of nonthermal radiofrequency stimulation on neuronal activity and neural circuit in mice. Adv. Sci. 10, 2205988.

Harward, S.C., Hedrick, N.G., Hall, C.E., Parra-Bueno, P., Milner, T.A., Pan, E., Laviv, T., Hempstead, B.L., Yasuda, R., McNamara, J.O., 2016b. Autocrine BDNF-TrkB signalling within a single dendritic spine. Nature 538, 99–103.

Harward, S.C., Hedrick, N.G., Hall, C.E., Parra-Bueno, P., Milner, T.A., Pan, E., Laviv, T., Hempstead, B.L., Yasuda, R., McNamara, J.O., 2016a. Autocrine BDNF–TrkB signalling within a single dendritic spine. Nature 538, 99–103.

Jiang, F., Tang, X., Tang, C., Hua, Z., Ke, M., Wang, C., Zhao, J., Gao, S., Jurczyszyn, A., Janz, S., 2021b. HNRNPA2B1 promotes multiple myeloma progression by increasing

AKT3 expression via m6A-dependent stabilization of ILF3 mRNA. J. Hematol. Oncol. 14, 1–5.
Jiang, S., Ma, Y., Shi, Y., Zou, Y., Yang, Z., Zhi, W., Zhao, Z., Shen, W., Chen, L., Wu, Y., 2024. Acute exposure of microwave impairs attention process by activating microglial inflammation. Cell Biosci. 14, 2.
Jiang, X., Liu, B., Nie, Z., Duan, L., Xiong, Q., Jin, Z., Yang, C., Chen, Y., 2021a. The role of m6A modification in the biological functions and diseases. Signal Transduct. Target. Ther. 6, 74.
Kaplan, S., Deniz, O.G., Önger, M.E., Türkmen, A.P., Yurt, K.K., Aydın, I., Altunkaynak, B.Z., Davis, D., 2006. Electromagnetic field and brain development. J. Chem. Neuroanat. 75, 52–61.
Lai, H., Levitt, B.B., 2022. The roles of intensity, exposure duration, and modulation on the biological effects of radiofrequency radiation and exposure guidelines. Electromagn. Biol. Med. 41, 230–255.
Leone, L., Cuccurazzu, B., Podda, M.V., Piacentini, R., Riccardi, E., Ripoli, C., Azzena, G. B., Grassi, C., 2011. Exposure to extremely low-frequency (50 Hz) electromagnetic fields enhances adult hippocampal neurogenesis in C57BL/6 mice. Clin. Neurophysiol. S162-S162.
Leone, L., Fusco, S., Mastrodonato, A., Piacentini, R., Barbati, S.A., Zaffina, S., Pani, G., Podda, M.V., Grassi, C., 2014. Epigenetic modulation of adult hippocampal neurogenesis by extremely low-frequency electromagnetic fields. Mol. Neurobiol. 49, 1472–1486.
Li, Y.-f., Chen, H.-x., Liu, Y., Zhang, Y.-z., Liu, Y.-q., Li, J., 2006. Agmatine increases proliferation of cultured hippocampal progenitor cells and hippocampal neurogenesis in chronically stressed mice. Acta Pharmacol. Sin. 27, 1395–1400.
Liu, J.J., Zhang, H.Y., Xin, C., Zhang, G.B., Lin, J.K., Hua, F., Chu, W.H., 2022. 20-hydroxyecdysone improves neuronal differentiation of adult hippocampal neural stem cells in high power microwave radiation-exposed rats. Biomed. Environ. Sci. 35, 504–517.
Maric, D., Maric, I., Chang, Y.H., Barker, J.L., 2003. Prospective cell sorting of embryonic rat neural stem cells and neuronal and glial progenitors reveals selective effects of basic fibroblast growth factor and epidermal growth factor on self-renewal and differentiation. J. Neurosci. 23, 240–251.
McCredden, J.E., Cook, N., Weller, S., Leach, V., 2022. Wireless technology is an environmental stressor requiring new underst anding and approaches in health care. Front. Public Health 10, 986315.
Mendelsohn, A.R., Larrick, J.W., 2006. Epigenetic-mediated decline in synaptic plasticity during aging. Rejuven. Res. 15, 98–101.
Minichiello, L., 2006. TrkB signalling pathways in LTP and learning. Nat. Rev. Neurosci. 10, 850–860.
Ouares, K.Ait, Beurrier, C., Canepari, M., Laverne, G., Kuczewski, N., 2019. Opto nongenetics inhibition of neuronal firing. Eur. J. Neurosci. 49, 6–26.
Owen, S.F., Liu, M.H., Kreitzer, A.C., 2019. Thermal constraints on in vivo optogenetic manipulations. Nat. Neurosci. 22, 1061–1065.
Pall, M.L., 2016. Microwave frequency electromagnetic fields (EMFs) produce widespread n europsychiatric effects including depression. J. Chem. Neuroanat. 75, 43–51.
Reichardt, L.F., 2006. Neurotrophin-regulated signalling pathways. Philos. Trans. R. Soc. B: Biol. Sci. 361, 1545–1564.
Sage, C., Burgio, E., 2017. Electromagnetic fields, pulsed radiofrequency radiation, and epigenetics: how wireless technologies may affect childhood development. Child Dev. 89, 129–136.
Schuderer, J., Kuster, N., 2003. Effect of the meniscus at the solid/liquid interface on the SAR distribution in Petri dishes and flasks. Bioelectromagn.: J. Bioelectromagn. Soc. Soc. Phys. Regul. Biol. Med. Eur. Bioelectromagn. Assoc. 24, 103–108.
Smith, M.P., Young, H., Hurlstone, A., Wellbrock, C., 2015. Differentiation of THP1 cells into macrophages for transwell co-culture assay with melanoma cells. Bio-Protocol 5 (e1638-e1638.
Tammen, S.A., Friso, S., Choi, S.-W., 2006. Epigenetics: the link between nature and nurture. Mol. Asp. Med. 34, 753–764.
Ueyama, E., Ukai, S., Ogawa, A., Yamamoto, M., Kawaguchi, S., Ishii, R., Shinosaki, K., 2011. Chronic repetitive transcranial magnetic stimulation increases hippocampal neurogenesis in rats. Psychiatry Clin. Neurosci. 65, 77–81.
Urnukhsaikhan, E., Mishig-Ochir, T., Kim, S.-C., Park, J.-K., Seo, Y.-K., 2006. Neuroprotective effect of low frequency-pulsed electromagnetic fields in ischemic stroke. Appl. Biochem. Biotechnol. 181, 1360–1371.
Vadodaria, K.C., Sebastian, J., 2014. Functional neurogenesis in the adult hippocampus: then and now. Front. Neurosci. 8, 55.
Vantini, G., Skaper, S.D., 2006. Neurotrophic factors: from physiology to pharmacology? Pharm. Res. 26, 1–15.
Wachs, F.-P., Couillard-Despres, S., Engelhardt, M., Wilhelm, D., Ploetz, S., Vroemen, M., Kaesbauer, J., Uyanik, G., Klucken, J., Karl, C., 2003. High efficacy of clonal growth and expansion of adult neural stem cells. Lab. Investig. 83, 949–962.
Wang, C.S., Kavalali, E.T., Monteggia, L.M., 2006. BDNF signaling in context: from synaptic regulation to psychiatric dis orders. Cell 185, 62–76.
Wang, H., Peng, R., Zhou, H., Wang, S., Gao, Y., Wang, L., Yong, Z., Zuo, H., Zhao, L., Dong, J., 2013. Impairment of long-term potentiation induction is essential for the disruption of spatial memory after microwave exposure. Int. J. Radiat. Biol. 89, 1100–1107.
Wang, H., Liu, Y., Sun, Y., Zhao, L., Dong, J., Xu, X., Wang, H., Zhang, J., Yao, B., Zhao, X., 2022. Changes in rat spatial learning and memory as well as serum exosome proteins after simultaneous exposure to 1.5 GHz and 4.3 GHz microwaves. Ecotoxicol. Environ. Saf. 243, 113983.
Wang, L., Chang, X., She, L., Xu, D., Huang, W., Poo, M.-m., 2016. Autocrine action of BDNF on dendrite development of adult-born hippoca mpal neurons. J. Neurosci. 35, 8384–8393.
Yarmolenko, P.S., Moon, E.J., Landon, C., Manzoor, A., Hochman, D.W., Viglianti, B.L., Dewhirst, M.W., 2011. Thresholds for thermal damage to normal tissues: an update. Int. J. Hyperth. 27, 320–343.
Yoshii, A., Constantine-Paton, M., 2010. Postsynaptic BDNF-TrkB signaling in synapse maturation, plasticity, and disease. Dev. Neurobiol. 70, 304–322.
Zhang, L., Nie, Q., Sun, X., 2006. BDNF-TrkB signaling is involved in the histopathological damage, synap tic protein loss and inflammatory response caused by an electromagneti c pulse in rat brain cortex. Neuroreport 30, 550–555.
Zhang, Y., Mao, R.-R., Chen, Z.-F., Tian, M., Tong, D.-L., Gao, Z.-R., Huang, M., Li, X., Xu, X., Zhou, W.-H., 2014. Deep-brain magnetic stimulation promotes adult hippocampal neurogenesis and alleviates stress-related behaviors in mouse models for neuropsychiatric disorders. Mol. Brain 7, 1–14.
Zhi, W.J., Peng, R.Y., Li, H.J., Zou, Y., Yao, B.W., Wang, C.Z., Liu, Z.H., Gao, X.H., Xu, X. P., Dong, J., 2018. Microwave radiation leading to shrinkage of dendritic spines in hippocampal neurons mediated by SNK-SPAR pathway. Brain Res. 1679, 134–143.